chemosensors

MDPI

Review

Integrated Photonic Sensors for the Detection of Toxic Gasses—A Review

Muhammad A. Butt * and Ryszard Piramidowicz

Institute of Microelectronics and Optoelectronics, Warsaw University of Technology, Koszykowa 75, 00-662 Warsaw, Poland

* Correspondence: ali.butt@pw.edu.pl

Abstract: Gas sensing is crucial for detecting hazardous gasses in industrial environments, ensuring safety and preventing accidents. Additionally, it plays a vital role in environmental monitoring and control, helping to mitigate pollution and protect public health. Integrated photonic gas sensors are important due to their high sensitivity, rapid response time, and compact size, enabling precise recognition of gas concentrations in real-time. These sensors leverage photonic technologies, such as waveguides and resonators, to enhance performance over traditional gas sensors. Advancements in materials and fabrication techniques could further improve their efficiency, making them invaluable for environmental monitoring, industrial safety, and healthcare diagnostics. In this review, we delved into photonic gas sensors that operate based on the principles of evanescent field absorption (EFA) and wavelength interrogation methods. These advanced sensing mechanisms allow for highly sensitive and selective gas detection, leveraging the interplay of light with gas molecules to produce precise measurements.

Keywords: gas sensor; integrated photonic sensor; evanescent field absorption; functional material

1. Introduction

Indoor and outdoor gas sensing is crucial for public health, safety, and environmental protection [1,2]. Indoors, gas sensors detect pollutants such as carbon monoxide (CO), volatile organic compounds (VOCs), and radon, which can reach hazardous levels and cause serious health issues like respiratory problems, neurological damage, or even fatalities [3]. Continuous indoor gas sensing ensures good air quality in homes, offices, and industrial buildings, verifying the effectiveness of ventilation systems and protecting occupants from toxic exposures. Outdoors, gas sensors monitor air quality and track emissions of harmful gasses like sulfur dioxide, nitrogen oxides, and ozone, which contribute to smog, acid rain, and climate change, negatively impacting ecosystems and human health [4]. These sensors help regulatory agencies enforce air quality standards, inform policy decisions, and increase public awareness of pollution levels. In industrial settings, both indoor and outdoor gas sensing is vital for detecting hazardous gas leaks, ensuring safe working conditions, and preventing environmental contamination [5]. Comprehensive gas sensing is therefore essential for protecting health, promoting environmental stewardship, and ensuring regulatory compliance across various sectors [6–11].

Metal oxide (MOX), catalytic, electrochemical gas sensors each have distinct mechanisms and applications, offering varied advantages and limitations. MOX sensors work by measuring changes in the electrical resistance of metal oxide materials when exposed to gasses [12,13]. They are robust, can detect a wide range of gasses, and operate well in harsh environments. However, they often require high operating temperatures and can suffer from drifting over time due to prolonged exposure to target gasses or environmental contaminants [14]. Catalytic gas sensors detect gasses by catalyzing a chemical reaction, usually combustion, on a heated element and measuring the resultant change in temperature or resistance [15–17]. These sensors are particularly effective for detecting combustible

check for updates

Citation: Butt, M.A.; Piramidowicz, R. Integrated Photonic Sensors for the Detection of Toxic Gasses—A Review. *Chemosensors* **2024**, *12*, 143. https://doi.org/10.3390/chemosensors12070143

Received: 11 June 2024
Revised: 5 July 2024
Accepted: 17 July 2024
Published: 18 July 2024

gasses like methane or hydrogen. They are reliable and have a fast response time, but they consume more power due to the need for continuous heating and are generally less sensitive to low gas concentrations [18]. Electrochemical sensors operate based on an electrochemical reaction between the target gas and an electrolyte, producing a current proportional to the gas concentration [19,20]. They are highly sensitive, selective, and capable of detecting low concentrations of gasses. Their low power consumption makes them suitable for portable applications [21,22]. However, they typically have a limited lifespan, are sensitive to environmental conditions such as temperature and humidity, and can be more expensive due to the materials used in their construction [19].

Integrated photonic sensors have revolutionized the field of gas sensing by leveraging the principles of photonics to provide highly sensitive, fast, and reliable recognition of various gasses [23–26]. These sensors utilize the interplay between light and gas molecules to identify and quantify gasses with exceptional precision [27]. The amalgamation of photonic components onto a single chip has significantly miniaturized gas sensors, making them more compact, energy-efficient, and cost-effective compared to traditional methods. This miniaturization is predominantly significant in products requiring portable or wearable devices, where size, weight, and power consumption are critical factors. The primary significance of gas sensing with integrated photonic sensors lies in their high sensitivity and specificity. Photonic sensors can detect minute concentrations of gasses, often in the parts-per-million (ppm) or parts-per-billion (ppb) range, which is essential for applications in environmental surveillance, industrial safety, and medical diagnostics [28]. For instance, detecting trace levels of dangerous gasses in industrial environments can avert accidents and ensure worker safety. In environmental monitoring, these sensors can track pollutants with high accuracy, contributing to better air quality management and public health [29–31]. In medical diagnostics, integrated photonic sensors can be used for non-invasive breath analysis to detect biomarkers for various diseases, enabling early diagnosis and personalized treatment.

Another significant advantage of integrated photonic sensors is their rapid response time and real-time monitoring capabilities. The interplay of light with gas molecules occurs at the speed of light, allowing for instantaneous detection and continuous monitoring of gas concentrations. This rapid response is crucial in scenarios where immediate detection is required, such as in detecting gas leaks or monitoring volatile organic compounds (VOCs) in industrial processes [32]. Additionally, the ability to provide real-time data enhances the effectiveness of monitoring systems, allowing for timely interventions and informed decision-making. Furthermore, the versatility and scalability of integrated photonic sensors make them suitable for a broad spectrum of uses. These sensors can be designed to target specific gasses by tuning the photonic components, such as lasers and waveguides (WGs), to the characteristic absorption wavelengths of the desired gasses [33]. This tunability, combined with the ability to integrate several sensing elements on a single chip, permits the simultaneous detection of multiple gasses, providing comprehensive monitoring solutions. The scalability of photonic integration also supports mass production, reducing costs and enabling widespread adoption in various industries.

The paper is organized as follows: Section 2 provides a brief description of indoor and outdoor toxic gasses and their impact on human health. Section 3 discusses the widely used optical WG architectures for gas sensing applications. The focus of the paper is on two gas sensing mechanisms, namely evanescent field absorption and the wavelength interrogation method, which are detailed in Section 4. Section 5 covers other types of photonic gas sensors, such as those based on metasurfaces, optical fibers, and photoacoustic spectroscopy. The fabrication methods for integrated photonic sensors are outlined in Section 6. Section 7 addresses the challenges and prospects of integrated photonic gas sensors. Finally, the paper concludes with a summary in Section 8.

2. Indoor and Outdoor Toxic Gasses

Indoor and outdoor environments both harbor a variety of toxic gasses that pose significant health risks to humans. Indoors, common toxic gasses include CO, which is produced by faulty furnaces, gas stoves, fireplaces, and tobacco smoke (Figure 1). Even at low levels, CO can cause headaches and dizziness, while high levels can be fatal [34]. Radon, a radioactive gas from the natural decay of uranium in the soil, infiltrates homes through cracks in floors and walls and is the leading cause of lung cancer among non-smokers [35]. VOCs, emitted from household products like paints, cleaning supplies, and furniture, can lead to respiratory issues, headaches, dizziness, and long-term health effects including cancer [36]. Nitrogen dioxide (NO_2), produced by combustion appliances like gas stoves and heaters, exacerbates asthma and reduces lung function [37]. Formaldehyde, found in building materials, tobacco smoke, and various household products, causes eye, nose, and throat irritation and is a known carcinogen. Ammonia (NH_3), released from cleaning products, textiles, and plastics, causes respiratory irritation, coughing, and throat irritation [38].

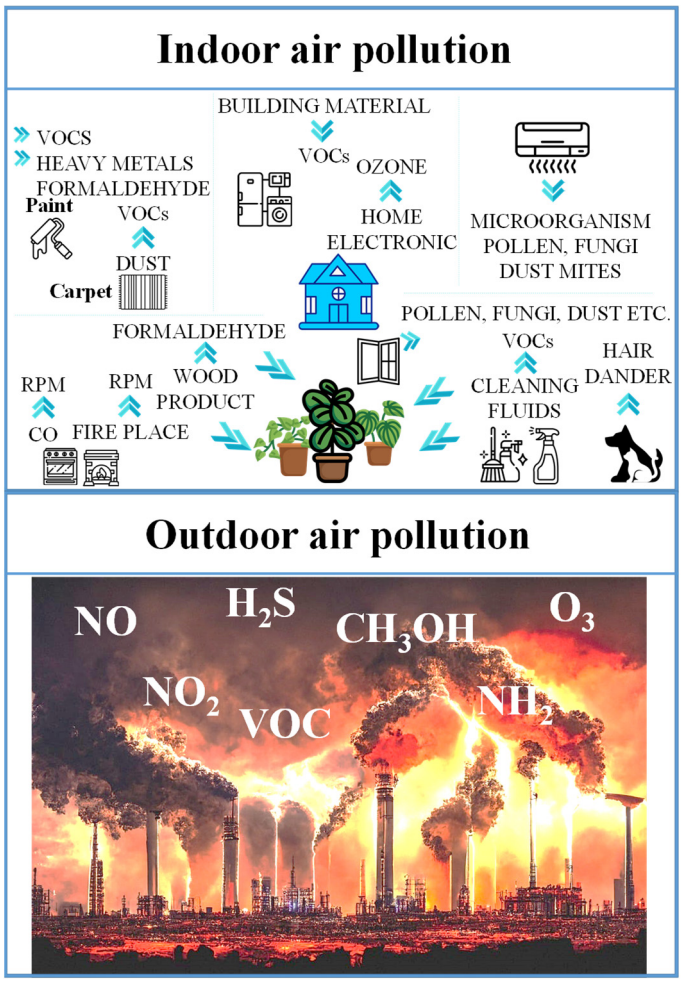

Figure 1. Graphical illustration depicting indoor (**Top**) and outdoor (**Bottom**) air pollution.

On the other hand, outdoor environments are similarly affected by toxic gasses. CO from vehicle exhaust and industrial processes can cause cardiovascular and neurological damage. NO_2, produced by vehicles, power plants, and industrial emissions, irritates the respiratory system and reduces lung function. Sulfur dioxide (SO_2), released from burning fossil fuels and industrial activities, causes respiratory problems and aggravates heart disease. Ozone (O_3), a secondary pollutant formed by chemical reactions between VOCs and nitrogen oxides (NO_x) in the presence of sunlight, leads to respiratory issues and

exacerbates asthma [39]. VOCs, emitted from industrial processes, vehicle exhausts, and chemical solvents, cause headaches, dizziness, and respiratory tract irritation, and some are carcinogenic [40]. Particulate matter (PM), though not a gas, carries adsorbed toxic gasses and fine particles (PM2.5) that penetrate deep into the lungs, causing cardiovascular and respiratory diseases and increasing mortality. Hydrogen sulfide (H_2S), produced by industrial activities and the decomposition of organic matter, causes respiratory irritation, headaches, and neurological damage [41]. NH_3, released from agricultural activities and industrial processes, irritates the respiratory system and eyes [42]. Benzene, a component of vehicle exhaust and industrial emissions, is a known carcinogen that causes leukemia and other blood disorders. Lead, emitted from industrial processes and historically from gasoline additives, causes neurological and developmental issues, particularly in children. Effective ventilation, emission controls, and regular supervising are crucial in mitigating the health risks associated with these harmful gasses, both indoors and outdoors.

3. Types of Optical WG Architectures Widely Used for Gas Sensing

WG architectures for gas sensors are ingeniously designed to maximize light–matter interplay, thereby enhancing sensitivity and enabling precise gas detection. One prominent architecture is the planar WG, where light is confined in a thin film on a substrate [43]. The evanescent field extends slightly beyond the WG, interacting with the surrounding gas [44]. This design can be further enhanced using materials with high refractive index contrasts, such as silicon (Si) or silicon nitride (SiN), which increase the strength of the evanescent field and thus improve sensitivity. Additionally, the surface of planar WGs can be functionalized with selective coatings to bind specific gas molecules, enhancing the sensor's selectivity and response [45]. The incidence of light on the edge of a glass coverslip for a microscope slide, deposited with a thin film on both faces, permitted the excitation of two resonances in each polarization state of the input light, TE and TM. This dually nanocoated WG was used for the simultaneous detection of two different parameters through further deposition of suitable materials on each face (Figure 2a) [46]. For instance, the detection of temperature and humidity was demonstrated using polydimethylsiloxane (PDMS) and agarose coatings, respectively, paving the way for the expansion of other dual-parameter sensors and even more parameters when each face of the coverslip is patterned. Additionally, the device was optimized to position two resonances in the near-infrared (NIR) and two resonances in the visible region, with sensitivities of 0.34 nm/°C and 0.23 nm/%RH in the visible region and 1.16 nm/°C and 0.34 nm/%RH in the NIR, respectively, showcasing the potential of the device for use in both spectral ranges and permitting the progress of sensors based on multiple resonances, each linked with a different parameter to be sensed [46].

Slot WGs and subwavelength grating (SWG) WGs are innovative structures that hold promise for gas sensing applications due to their exceptional properties. Slot WGs consist of a narrow slot between two high-index materials, typically Si or SiN, allowing for strong confinement of light in the slot region (Figure 2b) [47–50]. The E-field confinement in the slot WG is displayed in Figure 2c [51]. This confinement enhances the interplay between light and gas molecules, leading to increased sensitivity. Moreover, the slot region can be functionalized with materials that selectively bind target gas molecules, further enhancing the sensor's specificity.

SWG WGs, on the other hand, utilize periodic structures with feature sizes smaller than the wavelength of light, enabling precise control over the dispersion and confinement of light [52]. By engineering the grating parameters, such as period and duty cycle, the WG properties can be tailored to achieve desired sensing characteristics [53–55]. Both slot WGs and SWG WGs offer opportunities for highly sensitive and selective gas sensing platforms, holding potential for advancements in environmental surveillance, industrial process control, and healthcare diagnostics. A photonic array of resonant circular dielectric WGs with SWG was proposed as a robust and sensitive topological chemical sensor [56]. The device was tailored to identify trace amounts of a given chemical species through photonic edge modes, which are impervious to most sources of disorder. A simulation

in the MIR was performed, accounting for the absorption loss introduced by chemical molecules in contact with a strongly coupled photonic lattice of resonators. Due to the topological nature of the device, its chemical sensitivity scaled linearly with the system size, reaching the ppb range at the millimeter scale. These findings suggested that topological chemical sensors could allow the expansion of novel on-chip integrated photonic sensing technologies. An SWG WG was employed to enhance light–chemical interplay (Figure 2d). The strong coupling bridge resonator unit mediated the coupling between lattice sites in the array (Figure 2e). The design featured a dielectric circular array with designated source and drain for transmitting power. Gray rings represented lattice sites, while black rings indicated bridge resonators connecting these sites. All rings functioned as SWG WGs, as illustrated in the inset (Figure 2f). Red lines marked the topologically protected modes propagating along the edges of the array. The inset depicted a unit cell of the lattice [56].

Photonic crystal (PhC) WGs represent a highly sensitive architecture due to their ability to confine light in very small volumes [57,58]. These WGs consist of periodic dielectric structures that create photonic bandgaps, trapping and guiding light in defect regions (Figure 2g) [59]. The strong localization of light in these structures enhances the interplay with the gas molecules, leading to significant changes in the optical properties even with minute quantities of gas. Moreover, the PhC can be intended to operate at specific wavelengths where the target gas has strong absorption, further boosting the sensor's sensitivity [60–62]. Table 1 provides an overview of various WG architectures suitable for gas sensing applications, detailing their sensitivity and ease of fabrication.

Table 1. WG architectures for gas sensing: sensitivity and ease of fabrication.

WG Architecture	Description	Sensitivity	Ease of Fabrication
Planar WGs	Flat WGs typically fabricated on a substrate.	Moderate, limited interaction with evanescent field.	High, with well-established fabrication processes.
Rib WGs	WGs with a raised ridge structure on the substrate.	Enhanced compared to planar due to increased evanescent field.	Moderate, requires etching process.
Ridge WGs	Similar to rib WGs but with more pronounced confinement and elevation.	Higher sensitivity than rib WGs.	Moderate, requires etching process.
Slot WGs	Narrow slot between two high-index regions, creating strong field confinement.	High, strong interaction of the evanescent field in the slot.	Moderate, precise fabrication needed for narrow slot.
Plasmonic WGs	Utilize surface plasmon resonances at metal–dielectric interfaces for guiding light.	Very high, due to strong field enhancement at interfaces.	Complex, requires nanofabrication and precise metal deposition.
Hybrid Plasmonic WGs	Combine dielectric and plasmonic WGs to enhance field confinement and propagation length.	High, combining benefits of both dielectric and plasmonic fields.	Complex, advanced fabrication techniques for hybrid structures.
Subwavelength Grating WGs	Use periodic structures with subwavelength features for guiding light.	High, strong interaction with periodic structures.	Moderate to complex, requires precise control over grating patterns.
Suspended Membrane WGs	WGs suspended in air or another medium to maximize interaction with the environment.	Very high, maximum evanescent field exposure. Highly suitable for gas sensing.	Complex, requires suspension techniques and careful handling.

A suspended membrane WG for gas sensing is another advanced technology designed to enhance the detection and measurement of gas concentrations with high sensitivity and selectivity [63]. This WG consists of a thin, flexible membrane suspended over a substrate, allowing it to interact more directly with the surrounding gas molecules (Figure 2h) [64]. The membrane's material is typically chosen for its specific interaction properties with the target gas, and its suspended nature reduces background interference from the substrate,

improving detection accuracy [65]. When gas molecules adsorb onto the membrane, they induce changes in its optical or mechanical properties, such as refractive index or vibration frequency, which can be measured and correlated to gas concentration [64]. This configuration not only improves the sensor's sensitivity and response time but also enables miniaturization, making it suitable for portable and remote sensing purposes [66].

Surface plasmon (SP) WGs combine the advantages of plasmonics and WG technology to attain high sensitivity [67]. In these sensors, a metal layer, in general gold or silver, is integrated with a dielectric WG (Figure 2i) [68]. The interplay of light with the metal surface excites surface plasmons, which are highly sensitive to changes in the refractive index near the surface. When gas molecules adsorb onto the metal surface, they alter the local refractive index, shifting the surface plasmon resonance (SPR) condition. This shift can be detected with high precision, making SP WGs particularly effective for detecting low concentrations of gasses. Additionally, metal–insulator–metal (MIM) configurations [69] are also employed as highly sensitive WG structures (Figure 2j) [70].

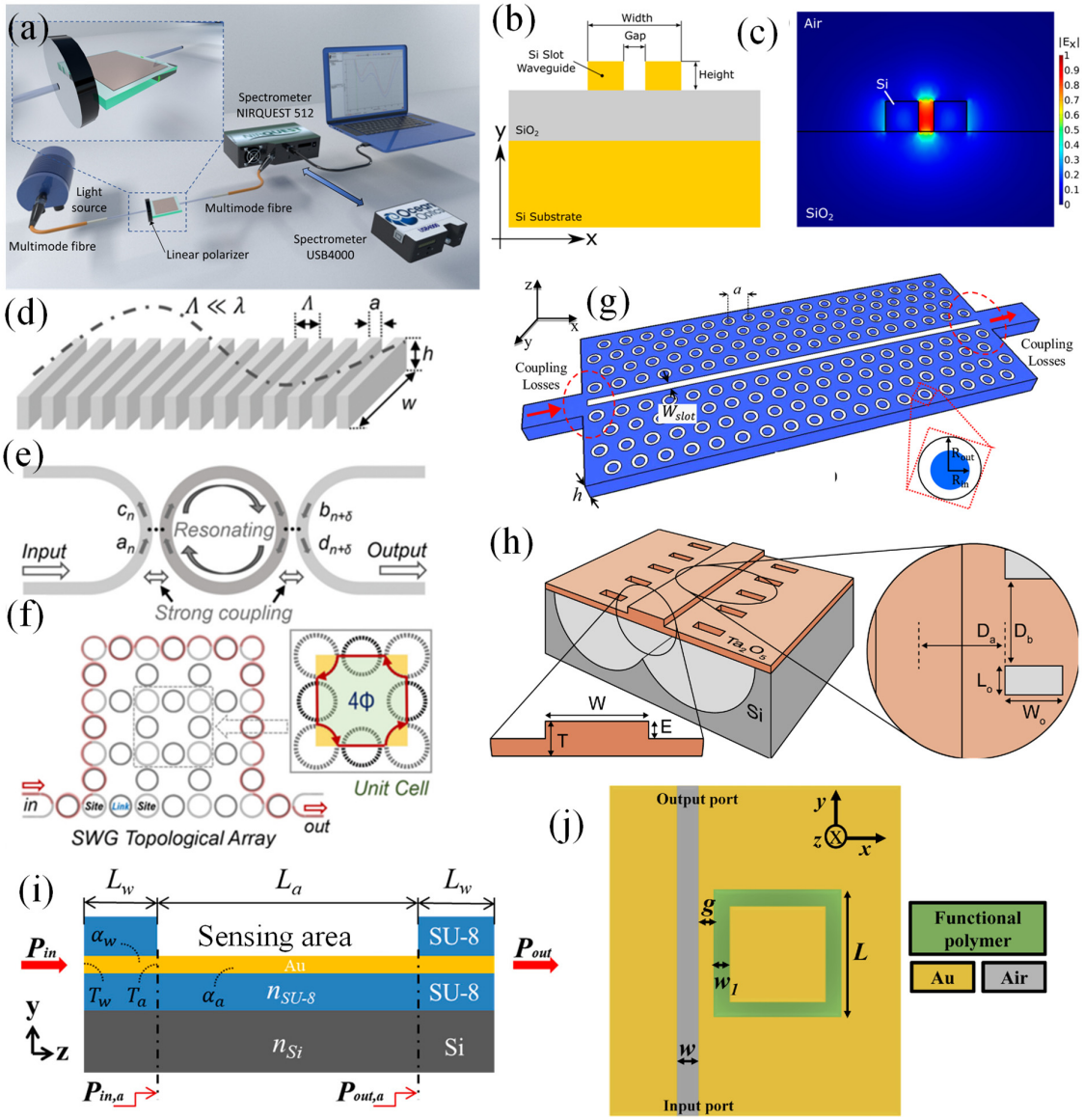

Figure 2. Different WG configurations for sensing purposes: (**a**) planar WG, (**b**) slot WG and E-field distribution (**c**) [51], (**d**) SWG WG [56], (**e**) ring resonator for coupling [56], (**f**) SWG WG-based ring resonator structures for sensing [56], (**g**) photonic crystal WG [59], (**h**) suspended membrane WG [64], (**i**) surface plasmon WG [68], (**j**) MIM WG [70].

4. Two Widely Employed Gas Sensing Mechanisms

Gas sensing mechanisms such as evanescent field absorption (EFA) and wavelength interrogation offer distinct yet complementary approaches to detecting gasses using optical WGs. When gas molecules are present near the WG surface, they interact with the evanescent field, leading to absorption at specific wavelengths characteristic of the gas. This absorption causes measurable changes in the light's intensity, which can be correlated to gas concentration [26,71]. On the other hand, the wavelength interrogation method involves observing shifts in the wavelength of light that resonate within the WG, often using structures like a Mach–Zehnder interferometer (MZI) [28] or ring resonators [72]. In this case, functional polymers like polyhexamethylene biguanide (PHMB) play a crucial role in enhancing the sensitivity and selectivity of gas sensors. When used in gas sensors, PHMB can be coated onto the surface of a sensing substrate, such as an optical WG [73,74]. Upon exposure to the target gas, PHMB undergoes changes in its physical or chemical properties, such as refractive index alteration, or conductivity variation. These changes can then be detected by the sensor's transduction mechanism—be it optical, electrical, or another modality—allowing for the precise quantification of the gas concentration [75]. The high affinity of PHMB for specific gasses, combined with its robustness and stability, makes it particularly effective for applications in environmental surveillance, industrial safety, and medical diagnostics, where accurate and reliable gas detection is paramount. Both mechanisms offer high sensitivity and specificity, making them valuable for applications ranging from environmental surveillance to industrial safety and medical diagnostics.

4.1. Gas Sensors Based on the Mechanism of EFA

The mid-infrared (MIR) region, typically defined as the wavelength range from 2.5 to 25 μm, is particularly significant for gas sensing applications due to its strong absorption characteristics for many molecular gasses [76,77]. The absorption wavelengths listed in Table 2 are representative of strong absorption peaks within the MIR region [76].

Table 2. Absorption wavelengths for various gasses in the MIR region.

Gas	Absorption Wavelengths (μm)	Absorption Wavenumbers (cm^{-1})
Carbon Dioxide (CO_2)	4.26, 14.99, 15.45	2349, 667, 648
Methane (CH_4)	3.31, 7.66	3020, 1305
Water Vapor (H_2O)	2.66, 6.27	3756, 1596
Nitrous Oxide (N_2O)	4.50, 7.80	2222, 1282
Ozone (O_3)	9.60, 14.24	1042, 702
Sulfur Dioxide (SO_2)	7.34, 8.72	1363, 1147
Ammonia (NH_3)	2.97, 9.22	3368, 1085
Carbon Monoxide (CO)	4.67	2143
Nitric Oxide (NO)	5.30, 5.44	1887, 1838
Formaldehyde (HCHO)	5.72, 9.60	1750, 1042

The actual absorption spectrum for each gas is broad and can contain many more peaks. In this spectral region, fundamental vibrational transitions of molecules occur, providing distinct and strong absorption features that can be used to identify and quantify various gasses with high sensitivity and specificity. Utilizing the MIR region for gas sensing enables the detection of a wide range of gasses, including CO_2, CH_4, and VOCs, which have critical absorption bands in this range. Advances in MIR sources, such as quantum cascade lasers, and detectors, like mercury cadmium telluride (MCT) photodiodes, have greatly enhanced the capabilities of MIR gas sensors. These technologies allow for real-time, in situ monitoring of gas concentrations, making them invaluable in environmental surveillance, industrial process control, and medical diagnostics, where precise and accurate gas detection is crucial.

Integrated photonic sensors utilizing the EFA mechanism represent a sophisticated approach to gas detection, leveraging the interplay between light and gas molecules at the interface of a WG [77]. In these sensors, light is guided through a photonic WG, and a small portion of the light, known as the evanescent field, extends beyond the surface of the WG

into the surrounding medium [78]. When gas molecules are present near the WG surface, they interact with this evanescent field, leading to absorption of specific wavelengths of light that correspond to the characteristic absorption spectra of the gas molecules [33,79,80].

Determining the evanescent field ratio (EFR) of a WG is vital for enhancing the performance and accuracy of gas sensors working on the principle of EFA [81]. The EFR quantifies the extent to which the optical field penetrates the neighboring gas medium outside the WG core. This penetration enables the sensor to detect variations in the gas's refractive index or absorbance, which are indicative of the presence and concentration of specific gas molecules. A higher EFR leads to a more significant interplay between the light and the gas, thereby improving the sensor's sensitivity and detection limit. Accurately determining this ratio allows for the optimization of the WG design and material properties to maximize the sensor's responsiveness and precision [26].

One of the primary advantages of using the EFA mechanism in integrated photonic sensors is the ability to perform real-time and continuous surveillance of gas concentrations [33,82]. The absorption of light by the gas molecules leads to a measurable change in the intensity or phase of the light propagating through the WG. This change can be detected and analyzed in real time, providing immediate feedback on the presence and concentration of the target gas. This capability is particularly valuable in applications such as industrial safety, where rapid detection of hazardous gasses can prevent accidents and ensure timely responses. Furthermore, integrated photonic sensors based on EFA can be miniaturized and integrated into compact, low-power devices. The use of photonic integration allows multiple sensing elements to be combined on a single chip, enabling multi-gas detection and reducing the overall footprint of the sensor system [83]. This miniaturization is advantageous for portable and wearable applications, where space and power are limited. Additionally, the robustness and stability of photonic WGs contribute to the durability and long-term reliability of these sensors, making them suitable for deployment in harsh environments.

Photonic gas sensors operating in the MIR region rely on specific material platforms to achieve efficient detection. Among the prominent materials are chalcogenide glasses, which offer wide transparency windows and high refractive indices, enabling the construction of compact and sensitive sensors. Another significant platform is silicon-on-insulator (SOI) [25], known for its compatibility with complementary metal oxide-semiconductor (CMOS) technology, facilitating the integration of photonic components with electronic circuits for enhanced functionality and performance. Additionally, III–V semiconductor materials like indium phosphide (InP) [84,85] and gallium arsenide (GaAs) [86] are utilized due to their superior optical properties and compatibility with laser sources, enabling direct on-chip integration of light sources and detectors. These material platforms play a fundamental role in the extension of robust and efficient photonic gas sensors for various applications ranging from environmental monitoring to industrial safety. Table 3 offers a comprehensive overview of various WG-based gas sensors operating on the principle of EFA mechanism. The evaluations of CH_4 gas sensors utilizing SOI technology, as illustrated in [33,87], have been thoroughly investigated. However, these studies have revealed a drawback beyond the wavelength of 3.6 μm, where the SiO_2 material experiences high absorption. Subsequently, the implementation of SOI-based WGs in the MIR region has become impractical. Given this limitation, alternative materials with a broad transparency range in the MIR region, as mentioned in [88–90], have emerged as feasible options. Materials such as Ge and CaF_2, characterized by high-index contrast, have been identified as promising substitutes for CH_4 gas sensing applications compared to SOI materials. For a thorough understanding of gas sensor evaluations for various gasses, significant contributions have been made in [91,92]. These investigations collectively enrich the broader field of gas sensing technologies, offering significant comprehensions into the diverse applications and material considerations necessary for enhancing sensor performance.

Optical structures fabricated using SOI technology offer an efficient platform for creating highly compact, versatile, and cost-effective devices. Yebo et al. demonstrated the

potential of this technology for integrated, low-power, and low-cost optical gas sensing. A room-temperature ethanol vapor sensor utilizing a ZnO nanoparticle film coating on a 5 μm radius SOI micro-ring resonator was presented in [92]. The local coating on the ring resonators was prepared from colloidal suspensions of ZnO nanoparticles approximately 3 nm in diameter. The porous nature of the coating provided a large surface area for gas adsorption. The refractive index changes in ZnO upon vapor adsorption shifted the resonance wavelength through evanescent field interaction. This sensing configuration detected ethanol vapor concentrations as low as 100 ppm, with an estimated detection limit below 25 ppm [92].

A multi-gas sensor system was developed by Dong et al., employing a single broadband light source and multiple pyroelectric detectors for CO, CO_2, and CH_4 [91]. This system utilized the time division multiplexing (TDM) technique. To facilitate and enhance multi-gas detection, a stepper motor-based rotating mechanism and a single-reflection spherical optical mirror were designed and implemented. Comprehensive measurements were conducted in both static detection mode (without rotation) and dynamic mode (with rotation) to evaluate the performance of the sensor system for detecting the three gas species. The influence of the motor's rotation period on sensor performance was also investigated, revealing that a rotation speed of 0.4π rad/s was necessary to achieve stable sensing performance, with a detection period of approximately 10 s for a full detection cycle. Allan deviation analysis indicated that the 1σ detection limits under static operation were 2.96 (parts per million in volume) ppmv for CO, 4.54 ppmv for CO_2, and 2.84 ppmv for CH_4. Under dynamic operation, the 1σ detection limits were 8.83 ppmv for CO, 8.69 ppmv for CO_2, and 10.29 ppmv for CH_4. This sensor showed promise for applications in various fields requiring the detection of CO, CO_2, and CH_4, such as in coal mines.

Jin et al. developed a chip-scale MIR sensor for detecting hydrocarbon gasses [93]. Fabricated using CMOS processes, the sensor utilized amorphous Si (a-Si) optical ridge WGs, as illustrated in Figure 3a. To assess the optical performance of these WGs, a MIR test station was setup, as shown in Figure 3b. The illumination source utilized was a pulsed laser operating at a 150 kHz repetition rate, with a pulse duration of 10 ns and an average power of 150 mW. A reflective lens collimated the probe light into a fluoride fiber featuring a 9 μm core and 125 μm cladding, which was subsequently butt-coupled into the WG. Precise alignment between the optical fiber and the a-Si WG was ensured using a microscope equipped with a long working distance 10× objective lens. The gas delivery system comprised three mass flow controllers (MFCs) to manage the flow rates of C_2H_2, CH_4, and N_2, adjusting the analyte concentration by modifying the gas flow ratios. The gas sample was introduced into a sealed PDMS chamber placed on top of the WG sensor, thereby exposing the a-Si WGs to the gas analytes. MIR signals emitted from the WGs were concentrated using a calcium fluoride biconvex lens with a 25 mm focal length and captured by a liquid nitrogen-cooled InSb camera. The WG exhibited a sharp fundamental mode throughout the λ = 2.70–3.50 μm range. Sensing performance was evaluated by measuring CH_4 and acetylene, identifying characteristic C–H absorption bands for CH_4 at λ = 3.29–3.33 μm and for acetylene at λ = 3.00–3.06 μm through spectral mode attenuation. Additionally, real-time surveillance of CH_4 and acetylene concentrations was demonstrated at λ = 3.02 and 3.32 μm. This MIR WG sensor thus enabled precise and instant analysis of hydrocarbon gas mixtures [93].

Two theoretical proposals for optical WG sensors based on slot WG and subwavelength slot (SWGS) WG utilizing SOS (silicon-on-sapphire) were introduced by Song et al. for CO_2 detection, as presented in Figure 3c,d [77]. The operational wavelength stands at 4.23 μm, corresponding to the maximal absorption line of CO_2. Power confinement factor (β) values exceed 40% and 50%, while propagation loss measures at 0.98 dB/cm and 2.99 dB/cm for the slot WG and SWGS WG, respectively. An inverted tapered structure facilitates the transition from strip WG to slot WG, constituting the sensing absorption region, with coupling efficiency exceeding 90%. Optimal absorption lengths for the slot

WG and SWGS WG are 1.02 cm and 0.33 cm, respectively, yielding maximum sensitivities of 6.66 × 10^{-5} (ppm^{-1}) and 2.60 × 10^{-5} (ppm^{-1}).

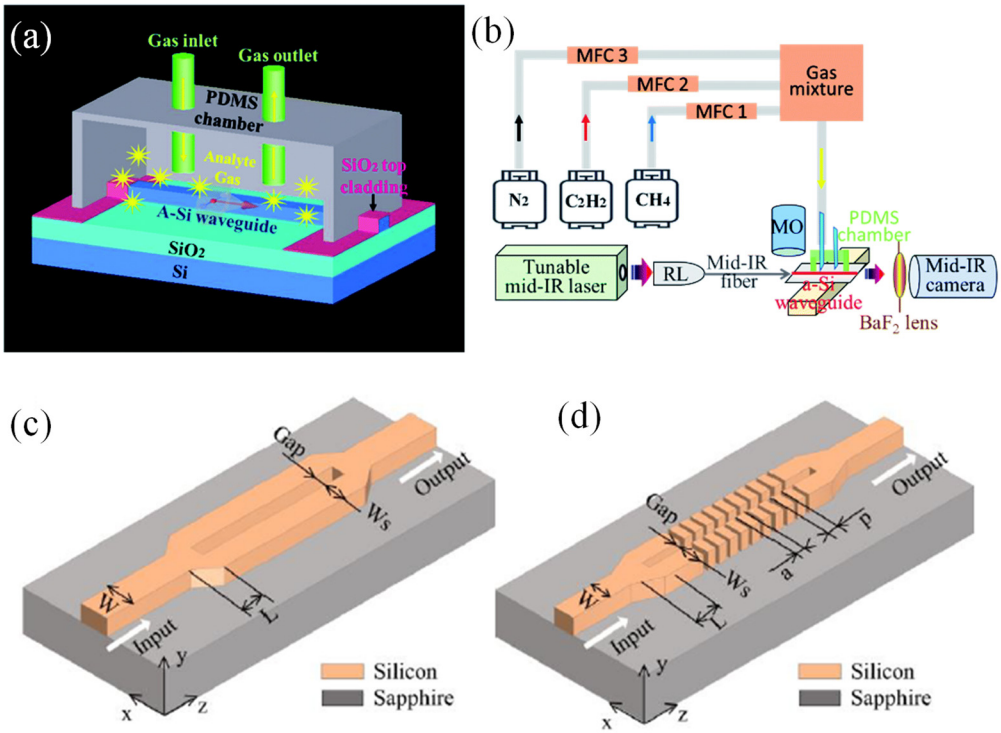

Figure 3. (**a**) Graphical illustration of a-Si ridge WG for hydrocarbon gas detection [93], (**b**) gas sensing setup [93], (**c**) slot WG structure [77], (**d**) subwavelength grating slot WG structure [77].

Kazanskiy et al. proposed a polarization-independent design for a hybrid plasmonic waveguide (HPWG) optimized at a 3.392 µm wavelength, corresponding to the absorption line of CH_4, as shown in Figure 4a [94]. This WG design demonstrated high mode sensitivity (S_{mode}) and EFR for both TE and TM hybrid modes. The modal analysis of the WG was conducted using two-dimensional (2D) and three-dimensional (3D) finite element methods (FEMs). At optimized WG parameters, the TE hybrid mode achieved S_{mode} and EFR values of 0.94 and 0.704, respectively, while the TM hybrid mode achieved S_{mode} and EFR values of 0.86 and 0.67, respectively. Additionally, both TE and TM hybrid modes exhibited a power dissipation of approximately 3 dB for a 20 µm long hybrid plasmonic WG at a 60% gas concentration. The inset of Figure 4a illustrates the field confinement for both TE and TM polarizations. The proposed WG scheme presented in this study is believed to overcome the limitations associated with polarization-controlled light, making it suitable for use in gas sensing applications.

Nanophotonic WGs have become central to a wide range of optical sensors. These structures channel light along specific paths on photonic chips, enabling light–matter interaction via an evanescent field. Despite their potential, WGs have yet to surpass free-space optics in sensitivity-critical applications like trace gas detection. The primary challenges hindering on-chip gas sensing include short optical path lengths, low interaction strengths, and spurious etalon fringes in spectral transmission. However, Vlk et al. proposed an MIR integrated WG sensor that addresses these issues effectively [82]. This sensor achieved a 107% evanescent field confinement factor in air, surpassing free-space beams in per-length optical interaction. Additionally, minimal facet reflections resulted in a flat spectral background and record-low absorbance noise, rivaling free-space spectroscopy. The sensor's performance was confirmed at 2.566 µm, demonstrating a 7 ppm detection limit for acetylene with just a 2 cm long WG. The WGs were evaluated in an end-fire coupling configuration employing the combined imaging and spectroscopy setup displayed in Figure 4b.

For the TM polarization, a WG propagation loss of 6.8 dB cm^{-1} was measured (Figure 4c,d). This loss was primarily due to light absorption in the Ta_2O_5 film caused by residual OH and water, and it is expected to decrease significantly with an optimized film deposition process [82].

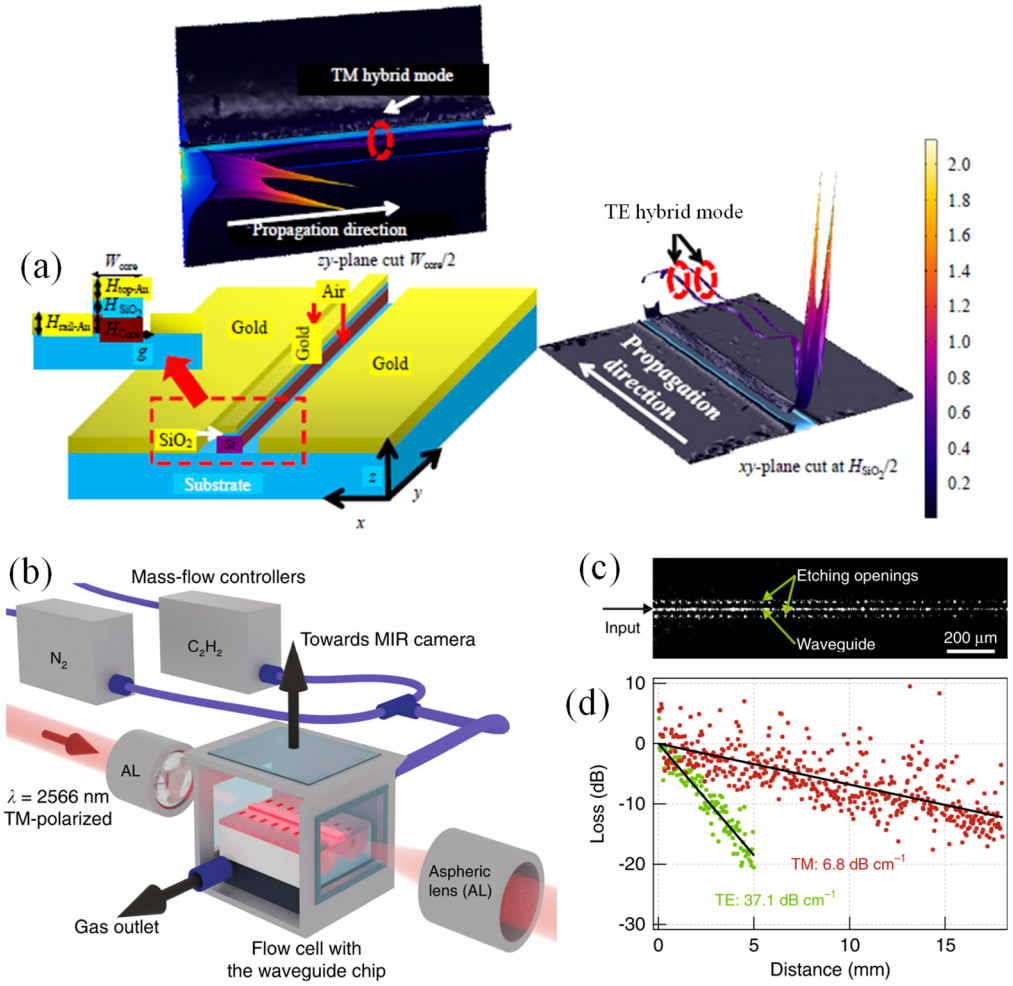

Figure 4. (**a**) Schematic representation of a polarization-independent HPWG structure [94], (**b**) outline of the experimental setup [82], (**c**) top-view MIR image of the WG at 2.566 µm, showing the guided mode visible through out-of-plane scattering at WG roughness and imperfections [82], (**d**) propagation loss determined from the decay of out-of-plane scattered light for both TM and TE polarizations. The TE mode, which is well confined in the Ta_2O_5 membrane, experiences higher loss due to material absorption compared to the strongly delocalized TM mode [82].

Table 3. Gas sensors based on different WG configurations working on the mechanism of EFA.

WG Configuration	Gas	Wavelength (µm)	EFR/Sensitivity/LOD	Ref.
Slot WG	N_2O	2.86	46%	[71]
HPWG	CH_4	3.392	3 dB power reduction for 60% of gas	[94]
Slot	CO_2	4.23	6.66 × 10^{-5} ppm^{-1}	[77]
SWGS	CO_2	4.23	2.60 × 10^{-5} ppm^{-1}	[77]
Suspended membrane WG	Athylene	2.566	7 ppm	[82]
Slot and double HPWG	CH_4	3.39	3 dB power decay for 20–22% of gas	[48]
Dual HPWG	CH_4	3.392	0.0715 mW/gas conc.	[79]
Strip WG	CO_2	4.26	14–16%	[83]
Ridge WG	CH_4	3.39	55%	[33]
Rib WG	CO	4.67	>30%	[95]

4.2. Gas Sensors Based on the Mechanism of Wavelength Interrogation Method

Photonic sensors based on the wavelength interrogation method represent a cutting-edge approach to gas detection, capitalizing on the interplay between light and gas molecules. This method encompasses monitoring shifts in the wavelength of light as it passes through or interacts with a gas sample [28]. Functional polymers that are sensitive to gas absorption play a crucial role in the development of advanced photonic gas sensors. These polymers are designed to interact specifically with certain gas molecules, causing changes in their physical or chemical properties upon gas absorption. Such changes can include alterations in refractive index, optical absorption, or fluorescence properties, which can be precisely detected using photonic methods. Polymers like polyhexamethylene biguanide (PHMB) [28,73,96–98], polyaniline (PANI) [99–101], polypyrrole (PPy) [102–104], and poly (ethylene oxide) (PEO) [105,106] have been extensively studied for their gas-sensitive properties. When integrated with photonic structures such as WGs or resonators, these polymers can significantly enhance the sensor's sensitivity and selectivity [70,74]. The gas-induced changes in the polymer can lead to detectable shifts in the light propagation characteristics within the photonic device. This interplay allows for real-time monitoring of gas concentrations with high accuracy. Moreover, functional polymers offer the advantage of tunability, where their chemical structure can be modified to target specific gasses, making them highly versatile for different sensing applications. Additionally, these polymers are often lightweight, cost-effective, and compatible with various substrates, facilitating their integration into compact and portable sensing platforms. Future research is focused on improving the stability and response time of these polymers, as well as exploring new polymer compositions and hybrid materials. Such advancements are expected to broaden the range of detectable gasses and enhance the overall performance of photonic gas sensors, making them indispensable tools for environmental monitoring, industrial safety, and healthcare diagnostics.

Mi et al. reported a Si photonic refractometric CO_2 gas sensor capable of detecting CO_2 at atmospheric concentrations and operating at room temperature [98]. This sensor employed a PHMB polymer that undergoes a reversible change in refractive index upon absorbing and releasing CO_2 molecules, functioning independently of humidity (see Figure 5a). The sensor's SEM image is depicted in Figure 5b. For the CO_2 sensing experiment, the chamber was preconditioned by flooding it with N_2 gas for 10 min. The initial resonance spectrum of the micro-ring resonator (MRR), centered around the 1.55 µm wavelength, is displayed by the black curve in Figure 5c. This spectrum revealed a loaded quality factor (Q factor) of 1.92×10^4 ($\pm$2%) for the MRR. Subsequently, 0.5% CO_2 gas was introduced into the chamber, and the resonance spectrum was measured again after 2 min once the sensor's response had stabilized. The presence of CO_2 gas resulted in the resonance spectrum shown by the red curve in Figure 5c, with a loaded Q factor of 1.87×10^4 ($\pm$2%), which matches the initial Q factor within experimental uncertainty. Thus, the two resonance spectra are nearly identical except for a small blue shift in the resonance wavelength. This shift indicates that CO_2 absorption reduces the refractive index of the PHMB polymer while having a minimal effect on optical absorption. This refractive index change is attributed to a redistribution of the electron density in the polymer's repeating units due to CO_2 molecule binding, altering its polarizability. The sensor detected CO_2 concentrations ranging from 0 to 500 ppm with a sensitivity of 6×10^{-9} (refractive index unit) RIU/ppm and a detection limit of 20 ppm. The MRR transducer offers a promising integrated solution for creating low-cost, compact CO_2 sensors, ideal for use in sensor networks for precise environmental monitoring of greenhouse gasses [98].

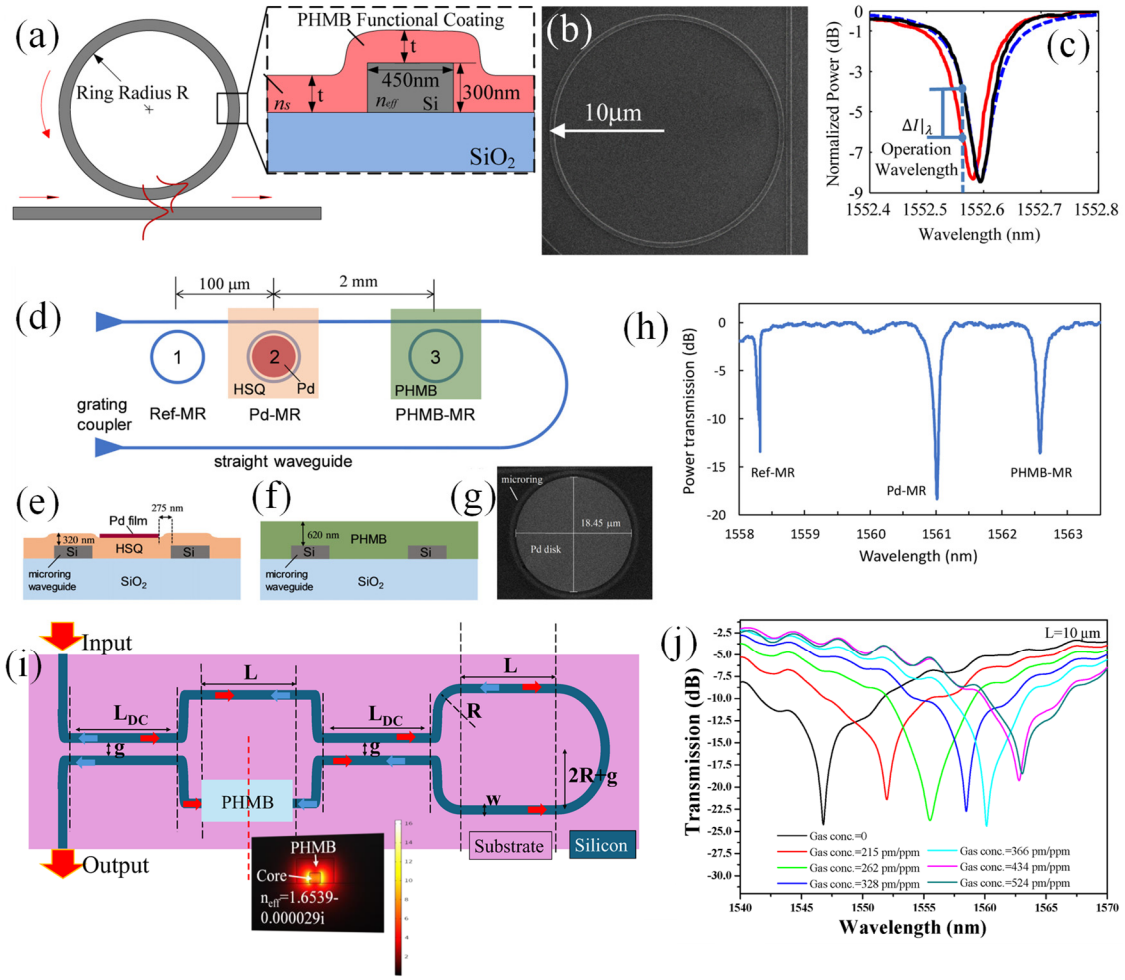

Figure 5. (**a**) Diagram of the Si MRR CO_2 gas sensor featuring a PHMB functional layer coating on the MRR WG [98], (**b**) SEM image of the Si MRR [98], (**c**) measured resonance spectrum of the functionalized MRR. The black curve represents the initial spectrum in pure N_2 gas, while the red curve shows the spectrum in the presence of a 0.5% CO_2 gas concentration. The blue dashed line indicates the resonance curve fit, which is used to correlate the transmitted powers to relative wavelength shifts [98]. (**d**) Schematic representation of the dual-gas sensor, comprising an array of three MRRs: Ref-MR for reference, Pd-MR for H_2 sensing, and PHMB-MR for CO_2 sensing. Cross-sectional diagrams illustrating [96] (**e**) the Pd functional layer and (**f**) the PHMB coating [96], (**g**) SEM image of the Pd-MR, (**h**) spectral response of the dual-gas sensor measured under N_2 gas flow conditions [96], (**i**) LT-MZI structure [28], (**j**) transmission spectrum of LT-MZI structure in the presence of varying CO_2 concentration [28].

A year later, Mi et al. introduced a Si photonic dual-gas sensor utilizing a wavelength-multiplexed MRR array for detecting both H_2 and CO_2 gasses simultaneously [96]. The schematic of this dual-gas sensor, depicted in Figure 5d, features an array of three MRRs evanescently coupled to a single straight WG. The sensor was built on an SOI substrate with a Si layer of 220 nm thickness on a 3 μm thick SiO_2 layer. The WG, designed to be 450 nm wide, supports a single TE mode with an effective index (n_{eff}) of 2.29 at the 1.55 μm wavelength. Microring 1, air-clad, acts as a reference sensor to monitor temperature and laser power variations. Microrings 2 and 3 serve as sensors for H_2 and CO_2 gasses, respectively, functionalized with Pd and PHMB, as revealed in the cross-sectional diagrams in Figure 5e,f. The SEM image of the Pd-MRR is presented in Figure 5g. Figure 5h shows the spectral response of the sensor chip after the test chamber was preconditioned by flooding it with N_2 gas for 10 min. The plot clearly shows three distinct resonances, each corresponding to one of the MRRs. Gas sensing experiments revealed that the PHMB-

functionalized MRR was highly sensitive to CO_2 gas and had excellent selectivity against H_2. Conversely, the Pd-functionalized MRR showed sensitivity to both H_2 and CO_2 gasses, making it unsuitable for detecting H_2 in a CO_2-containing gas mixture. The dual-gas sensing approach was shown to enable accurate measurement of H_2 concentration in the presence of CO_2 by compensating for the cross-sensitivity of Pd to CO_2.

In a recent study, M.A. Butt conducted a numerical analysis on the loop-terminated Mach–Zehnder interferometer (LT-MZI) structure aimed at CO_2 gas detection applications (Refer to Figure 5i [28]). The sensing arm was treated with a PHMB polymer, known for its high sensitivity and selectivity to CO_2 gas. When CO_2 gas was absorbed, it led to a reduction in the refractive index of the host material, which caused a shift in the interference pattern of the LT-MZI structure. This shift resulted in a redshift in the device's transmission spectrum, as illustrated in Figure 5j. The device demonstrated sensitivities of 7.63 pm/ppm, 34.46 pm/ppm, and 74.78 pm/ppm for sensing arm lengths of 5 μm, 10 μm, and 15 μm, respectively. Although increasing the sensitivity is possible, it would require a larger device size. This advanced sensor design enabled the detection of a wide range of CO_2 gas concentrations from 0 to 524 ppm. The device, being both compact and highly sensitive, is a crucial tool for monitoring indoor CO_2 levels, thereby fostering a healthier breathing environment for occupants. Table 4 summarizes the significant reports on WG-based gas sensors working on the principle of the wavelength interrogation method.

Table 4. Recently proposed integrated photonic gas sensors based on different designs working on the principle of wavelength interrogation method.

Platform	Sensor Design	Sensing Material	Gas	Sensitivity/LOD	Ref.
SOI	MRR array	Pd and PHMB	H_2 and CO_2	9.15×10^{-4} pm/ppm for H_2 and 1.44×10^{-3} pm/ppm for CO_2	[96]
SOI	RR	PbSe	CO_2	10 ppm	[107]
SOI	RR	-	VOC	1.7 pm/1000 ppm	[108]
SOI	LT-MZI structure	PHMB	CO_2	74.78 pm/ppm	[28]
Plasmonic	MIM WG based square ring cavity	PHMB	CO_2	135.95 pm/ppm	[70]
Plasmonic	MIM WG based E-shaped cavity	Methane sensitive membrane	CH_4	−12.017 nm/%	[109]

5. Other Kinds of Photonic Gas Sensors

Apart from integrated photonic gas sensors, several other widely used photonic gas sensors are discussed in this section. These include metasurface (MS)-based gas sensors, optical fiber-based gas sensors, and photoacoustic spectroscopy (PAS) gas sensors. Each of these technologies leverages unique photonic principles to achieve high sensitivity and selectivity in gas detection. Together, these photonic gas sensor technologies are crucial in various applications, including environmental monitoring, industrial safety, and medical diagnostics, pushing the boundaries of gas detection capabilities.

5.1. MS-Based Gas Sensors

MS-based gas sensors leverage engineered surfaces with sub-wavelength structures to manipulate light in novel ways, enhancing gas detection capabilities [110–112]. These MSs are composed of an array of nanostructures that can modify the phase, amplitude, and polarization of light, enabling highly sensitive and selective detection of gasses [113,114]. Nanostructures can be designed to support resonant modes that enhance the interplay between light and gas molecules, thereby increasing the sensitivity of the sensor. When a gas molecule adsorbs the functional polymers deposited onto the MS, it causes a measurable shift in the resonant frequency or intensity of the transmitted or reflected light, which can be correlated with the gas concentration [73,111]. MS-based gas sensors are advantageous due to their ultra-thin profiles, which enable integration into compact devices, and

their ability to operate across a wide range of wavelengths, including the visible and IR regions [115]. These sensors are particularly useful for detecting trace amounts of gasses in environmental monitoring, industrial process control, and medical diagnostics [116]. The flexibility in designing the nanostructures enables the tuning of the sensor's response to specific gasses, providing high selectivity and sensitivity [117]. Additionally, progress in assembly methods, such as electron beam lithography (EBL) and nanoimprint lithography (NIL), has facilitated the mass production of MS-based sensors, making them a promising technology for widespread gas sensing applications [118].

5.2. Optical Fiber-Based Gas Sensors

Optical fiber-based gas sensors utilize the properties of light transmission through optical fibers to detect and measure gas concentrations [30]. These sensors operate on various principles, including absorption spectroscopy, fluorescence, and surface plasmon resonance (SPR). In absorption spectroscopy-based optical fiber sensors, light transmitted through or along a gas-sensitive fiber segment is attenuated at specific wavelengths where the gas absorbs light [119,120]. This attenuation is used to determine the gas concentration. Fluorescence-based sensors involve the interplay of the target gas with a fluorescent material coated on or incorporated into the fiber [121–123]. The gas-induced changes in fluorescence intensity or wavelength shift are measured to quantify the gas concentration [124,125]. SPR-based optical fiber sensors employ a metal-coated fiber where the interplay of light with the metal surface excites surface plasmons, which are sensitive to changes in the refractive index near the fiber surface caused by gas adsorption [126,127]. Optical fiber sensors are highly sensitive, offer real-time monitoring, and can be deployed in harsh environments due to their robustness and resistance to electromagnetic interference. They are widely used in applications such as industrial safety monitoring, environmental pollution detection, and medical diagnostics. The ability to perform remote sensing and multiplexing, where multiple sensors are integrated into a single fiber, further enhances their utility in various gas sensing scenarios [128,129].

5.3. Photoacoustic Spectroscopy (PAS) Gas Sensors

Photoacoustic spectroscopy (PAS) gas sensors exploit the photoacoustic effect to detect gas concentrations with high sensitivity and selectivity [130,131]. In PAS, modulated light is absorbed by gas molecules, causing periodic heating and cooling, which generates pressure waves or acoustic signals. These pressure waves are detected by highly sensitive microphones or quartz tuning forks. The amplitude of the acoustic signal is proportional to the gas concentration, allowing for precise quantification of trace gasses. PAS sensors can operate across a wide range of wavelengths, from UV to IR, making them versatile for detecting various gasses [132–134]. The key advantages of PAS sensors include their ability to provide real-time measurements, their high sensitivity, which can reach ppb levels, and their minimal interference from other gasses, as the detection is based on the unique absorption characteristics of the target gas [135]. PAS technology is particularly effective in detecting gasses such as CO_2, CH_4, and VOCs. The development of compact, portable PAS sensors has expanded their use in field applications, providing a powerful tool for on-site gas analysis [136]. Advances in laser technology, such as the use of quantum cascade lasers (QCLs) [136], have further enhanced the sensitivity and selectivity of PAS sensors, making them an indispensable technology for modern gas sensing [137].

6. Research towards Developing Commercial Gas Sensor Products

For gas sensors to achieve commercial success, they must excel in sensitivity, selectivity, longevity, cost-effectiveness, and measurement speed. Integrated optical sensors, particularly those targeting ammonia, offer a promising solution [138]. These sensors retain the benefits of optical detection while potentially reducing costs and minimizing the footprint compared to existing commercial products. Photonic integrated circuits (PICs) are particularly well-suited for environmental and agricultural monitoring due to their small

size and scalability. These attributes make it feasible to deploy extensive sensor networks. Current technological advancements, especially in indium phosphide-based commercial foundries, have reached the maturity needed to detect ammonia at concentrations below 100 ppb. Despite this progress, the market still lacks portable, low-cost ammonia sensors capable of such sensitivity, which hinders widespread emission monitoring, such as in pig farms. To assess the feasibility of these sensors, an analysis was conducted using standard noise figures from multiproject wafer platforms operating around the 1550 nm wavelength. This study was further extended to include other gasses with absorption features near telecom wavelengths, demonstrating the broad potential of these sensors for various applications [138].

Hansel et al. introduced a fully integrated optical ammonia sensor utilizing a PIC equipped with a tunable laser source and a hollow-core fiber (HCF) serving as the gas interaction cell [139]. This PIC also incorporated a photodetector capable of recording the absorption signal within the same device. The sensor was designed to target an ammonia absorption line at 1522.45 nm, achievable with indium phosphide-based, telecom-compatible PICs. The setup included a 1.65 m long HCF connected at both ends to a single-mode fiber (SMF) using a mechanical splice, enabling rapid filling and purging of the fiber within minutes. As a proof of concept, the detection of a 5% ammonia gas concentration was demonstrated, showcasing the sensor's capability and its potential to detect significantly lower concentrations. This development represents a significant step towards creating low-cost, integrated, and portable gas sensors with broad applications in environmental gas sensing.

7. Fabrication Methods of Integrated Photonic Sensors

The fabrication of integrated photonic devices, including sensors, involves several sophisticated techniques that enable the miniaturization and integration of optical components onto a single chip [140]. These methods leverage advancements in materials science, nanotechnology, and semiconductor processing to create devices that can manipulate light with high precision and efficiency. One of the primary methods used in the fabrication of integrated photonic devices is photolithography [141]. This process involves transferring a geometric pattern from a photomask to a light-sensitive chemical photoresist layer on the substrate. The exposed areas of the photoresist are then developed, revealing the underlying substrate, which can be etched away to create the desired structures. Photolithography can produce features with dimensions in the order of nanometers, essential for the intricate designs required in photonic circuits.

Another critical fabrication technique is chemical vapor deposition (CVD). CVD is used to deposit thin films of materials, such as SiO_2 or SiN, which are essential for WGs that channel light in photonic devices [142]. In this process, gaseous precursors react on the substrate surface to form a solid film. Variations in CVD, such as plasma-enhanced CVD (PECVD), can offer better control over film properties and deposition conditions, which is crucial for achieving high-quality optical components. Techniques such as atomic layer deposition (ALD) and molecular beam epitaxy (MBE) are used for the precise deposition of ultra-thin films and the growth of high-quality crystalline layers, respectively [143]. ALD allows for the deposition of conformal layers with atomic-level control, which is beneficial for creating multilayer structures and coatings with precise thicknesses [142]. MBE is used to grow epitaxial layers of materials, often with tailored electronic and optical properties, which are critical for the performance of photonic devices.

Alternatively, the sol–gel method combined with dip-coating processes offers a promising avenue for the development of low-cost photonic sensors [144]. The sol–gel technique involves the synthesis of inorganic materials from molecular precursors, typically metal alkoxides, via a solution-based route. This method allows for precise control over material composition, structure, and morphology, facilitating the customization of sensor properties. By employing dip-coating, thin films of the synthesized sol–gel materials can be uniformly deposited onto substrates, enabling the fabrication of sensor coatings with

tailored thickness and optical characteristics. This approach not only minimizes material wastage but also reduces production costs associated with traditional deposition techniques. Furthermore, the simplicity and scalability of sol–gel processing make it accessible for mass production, contributing to the affordability of photonic sensors without compromising performance [145]. Table 5 offers a comprehensive comparison of deposition methods and their characteristic features.

Table 5. Different deposition methods and their characteristics.

Deposition Method	Features	Cost	Materials	Film Quality
CVD	Uses chemical reactions of vapor-phase precursors at elevated temperatures.	Moderate to High	Semiconductors, dielectrics, metals	High-quality, uniform films with good adhesion.
PECVD	Utilizes plasma to enhance chemical reactions, allowing for lower temperatures.	Moderate to High	Dielectrics, semiconductors	High-quality films, often with improved properties due to plasma.
ALD	Sequential self-limiting reactions for precise thickness control at atomic scale.	High	Oxides, nitrides, metals, semiconductors	Extremely high-quality, ultra-thin, and uniform films.
MBE	Uses a beam of atoms or molecules directed at the substrate in an ultra-high vacuum.	Very High	Semiconductors, oxides	Very high-quality, crystalline films with atomic precision.
Dip-Coating Process	Substrate is dipped into a solution and then withdrawn at a controlled rate to form a thin film.	Low	Polymers, oxides, glasses	Variable quality, dependent on solution properties and withdrawal speed.

Conventional photolithography and electron beam lithography (EBL) are both advanced microfabrication techniques, each with unique strengths and limitations. Photolithography employs ultraviolet (UV) light to transfer patterns from a photomask onto a photoresist layer, facilitating large-scale patterning at high throughput and relatively low cost [146]. This method is effective for creating features ranging from several micrometers to sub-micrometer sizes [147]. In contrast, EBL uses a focused beam of electrons to directly write patterns onto a substrate with exceptional precision, achieving feature sizes as small as a few nanometers [148,149]. While EBL offers unparalleled resolution and design flexibility, it operates at slower speeds and higher costs compared to UV photolithography. Both techniques are indispensable in semiconductor manufacturing, nanotechnology research, and the advancement of optical and electronic devices, each selected based on specific needs for resolution, throughput, and economic feasibility. Etching processes, including both dry etching (such as reactive ion etching (RIE)) and wet etching, are employed to remove material and define the final geometry of the photonic devices [150,151]. Dry etching uses plasma to etch away material in a highly controlled manner, allowing for anisotropic etching profiles essential for vertical sidewalls in WGs. Wet etching, on the other hand, uses liquid chemicals to selectively dissolve materials, which can be more suitable for certain materials and applications.

8. Challenges and Prospects

Integrated photonic gas sensors represent a promising frontier in gas sensing technology, leveraging the advantages of photonics to achieve high sensitivity, selectivity, and miniaturization. These sensors integrate photonic circuits on a single chip to detect

and measure gas concentrations, using light–matter interactions. However, despite their potential, several challenges need to be addressed to realize their full capabilities and widespread adoption. The selectivity of photonic gas sensors poses significant challenges in their practical implementation. One primary concern is the interference from other gasses present in the environment, which can lead to false readings or inaccurate detection. Achieving high selectivity requires sensor designs that can discriminate between target gasses and potential interferents effectively. Additionally, variations in environmental conditions such as temperature and humidity can further complicate selectivity, as they may influence the sensor's response to different gasses. Developing robust algorithms for signal processing and pattern recognition is essential to enhance the selectivity of photonic gas sensors, enabling reliable and accurate detection in real-world applications.

Another major concern is the fabrication and integration complexity. Creating integrated photonic circuits that can precisely and reliably detect gasses requires advanced manufacturing techniques, often involving sophisticated lithography and material deposition processes [152]. Ensuring consistent quality and performance across large-scale production adds another layer of difficulty. Additionally, integrating various components, such as light sources, WGs, detectors, and gas-sensitive materials, into a single compact device without compromising performance remains a significant engineering challenge. Another critical issue is the sensitivity and selectivity of the sensors. While photonic gas sensors can achieve high sensitivity due to their interaction with light, distinguishing between different gas species accurately can be problematic [153]. This is because many gasses may exhibit similar optical absorption features, leading to cross-sensitivity and potential false readings [154]. Developing materials and sensor designs that enhance selectivity, possibly using functionalized surfaces or advanced signal processing algorithms, is essential to overcome this challenge [155].

Ensuring the stability of photonic gas sensors is crucial for their reliable and long-term operation. One significant issue is the drift in sensor response over time, which can result from factors such as aging of sensor materials, variations in manufacturing processes, and exposure to environmental conditions. Drift can lead to a decrease in sensor accuracy and sensitivity, impacting the reliability of gas detection. Maintaining stability often requires careful calibration and periodic recalibration of the sensor to correct for any deviations in its response. Furthermore, efforts to enhance the stability of photonic gas sensors may involve the use of robust materials, protective coatings, and advanced encapsulation techniques to minimize the effects of environmental factors and ensure consistent performance over extended periods.

The limit of detection (LOD) presents a critical challenge for photonic gas sensors, influencing their effectiveness in detecting trace amounts of target gasses. Achieving low LODs is essential, particularly in applications where detecting very low concentrations of gasses is necessary for safety or environmental monitoring. However, several factors can limit the LOD of photonic gas sensors, including inherent noise in the sensor system, background interference from other gasses, and limitations in the sensor's sensitivity and dynamic range. Improving the LOD often involves optimizing sensor design parameters, such as the selection of appropriate sensing materials, enhancing signal-to-noise ratios through advanced signal processing techniques, and minimizing cross-sensitivity to non-target gasses [156]. Additionally, advancements in nanotechnology and materials science have opened new avenues for enhancing the sensitivity and selectivity of photonic gas sensors, potentially pushing the LOD to even lower levels [157].

Despite these obstacles, the prospects for integrated photonic gas sensors are promising. Advances in material science, such as the development of novel nanomaterials and metamaterials, offer pathways to enhance sensor performance [110,111,116,117,158]. These materials can be engineered to have specific interactions with certain gas molecules, improving both sensitivity and selectivity. Moreover, the integration of photonic sensors with complementary technologies, such as microelectromechanical systems (MEMSs) and

microfluidics, can lead to the development of multifunctional sensing platforms that are compact, robust, and capable of real-time monitoring.

In terms of applications, integrated photonic gas sensors have the potential to revolutionize fields such as environmental monitoring, industrial process control, and healthcare [96]. For instance, they could provide real-time, on-site monitoring of air quality with unprecedented precision, helping to address environmental and public health concerns [159]. In industrial settings, these sensors could be used for the continuous monitoring of hazardous gasses, improving safety and operational efficiency. In healthcare, they could enable non-invasive diagnostics through the detection of biomarkers in one's breath, offering a new avenue for early disease detection.

9. Concluding Remarks

Gas sensing plays a vital role in ensuring safety and prevention by detecting harmful gasses before they reach dangerous levels. In industrial settings, gas sensors can identify leaks of toxic or flammable gasses, preventing explosions and protecting workers from poisoning. In homes and commercial buildings, they can detect carbon monoxide, providing early warnings that prevent fatalities. Additionally, gas sensing is critical in disaster prevention, such as detecting methane leaks in mining operations to avert explosions. By providing real-time monitoring and alerts, gas sensing technologies significantly enhance safety and prevent accidents in various environments. Integrated photonic gas sensors have demonstrated significant advancements in sensitivity, selectivity, and miniaturization, offering a robust platform for real-time and on-site gas detection. These sensors leverage the principles of photonic integration to enhance performance and reduce the size and cost of traditional gas sensing systems.

The successful integration of various photonic components on a single chip has enabled the detection of multiple gasses simultaneously with high precision. Looking forward, the future of integrated photonic gas sensors is promising, with ongoing research focused on further enhancing their sensitivity, expanding their detection range, and improving their robustness in diverse environmental conditions. Advances in materials science, nanofabrication techniques, and data processing algorithms are expected to play crucial roles in these developments. Additionally, the integration of these sensors with the Internet of Things (IoT) could revolutionize environmental monitoring, industrial safety, and healthcare applications by providing continuous, real-time monitoring and analysis of gas compositions.

Author Contributions: Conceptualization, M.A.B.; methodology, M.A.B.; software, M.A.B.; validation, M.A.B. and R.P.; formal analysis, M.A.B.; investigation, M.A.B.; resources, R.P.; data curation, M.A.B.; writing—original draft preparation, M.A.B.; writing—review and editing, M.A.B. and R.P.; visualization, M.A.B.; supervision, R.P.; project administration, R.P.; funding acquisition, M.A.B. All authors have read and agreed to the published version of the manuscript.

Funding: This research received no external funding.

Acknowledgments: The author acknowledges the constant support of Warsaw University of Technology in the completion of this work.

Conflicts of Interest: The authors declare no conflicts of interest.

References

1. Wang, J.; Viciano-Tudela, S.; Parra, L.; Lacuesta, R.; Lloret, J. Evaluation of Suitability of Low-Cost Gas Sensors for Monitoring Indoor and Outdoor Urban Areas. *IEEE Sens. J.* **2023**, *23*, 20968–20975. [CrossRef]
2. Yang, L.; Zheng, G.; Cao, Y.; Meng, C.; Li, Y.; Ji, H.; Chen, X.; Niu, G.; Yan, J.; Xue, Y.; et al. Moisture-resistant, stretchable NO_x gas sensors based on laser-induced graphene for environmental monitoring and breath analysis. *Microsyst. Nanoeng.* **2022**, *8*, 78. [CrossRef] [PubMed]
3. Lee, J.; Jung, Y.; Sung, S.H.; Lee, G.; Kim, J.; Seong, J.; Shim, Y.-S.; Jun, S.C.; Jeon, S. High-performance gas sensor array for indoor air quality monitoring: The role of Au nanoparticles on WO_3, SnO_2, and NiO-based gas sensors. *J. Mater. Chem. A* **2021**, *9*, 1159–1167. [CrossRef]

4. Cao, J.; Chen, Q.; Wang, X.; Zhang, Q.; Yu, H.D.; Huang, X.; Huang, W. Recent Development of Gas Sensing Platforms Based on 2D Atomic Crystals. *Research* **2021**, *2021*, 9863038. [CrossRef] [PubMed]
5. Kendler, S.; Zuck, A. The Challenges of Prolonged Gas Sensing in the Modern Urban Environment. *Sensors* **2020**, *20*, 5189. [CrossRef] [PubMed]
6. Yaqoob, U.; Younis, M.I. Chemical Gas Sensors: Recent Developments, Challenges, and the Potential of Machine Learning—A Review. *Sensors* **2021**, *21*, 2877. [CrossRef] [PubMed]
7. Liu, X.; Cheng, S.; Liu, H.; Hu, S.; Zhang, D.; Ning, H. A Survey on Gas Sensing Technology. *Sensors* **2012**, *12*, 9635–9665. [CrossRef] [PubMed]
8. Padvi, M.N.; Moholkar, A.V.; Prasad, S.R.; Prasad, N.R. A Critical Review on Design and Development of Gas Sensing Materials. *Eng. Sci.* **2021**, *15*, 20–37. [CrossRef]
9. Eranna, G.; Joshi, B.C.; Runthala, D.P.; Gupta, R.P. Oxide Materials for Development of Integrated Gas Sensors—A Comprehensive Review. *Crit. Rev. Solid State Mater. Sci.* **2004**, *29*, 111–188. [CrossRef]
10. Sihag, S.; Dahiya, R.; Rani, S.; Berwal, P.; Jatrana, A.; Sisodiya, A.K.; Sharma, A.; Kumar, V. Low ppm NO_2 detection through advanced ultrasensitive copper oxide gas sensor. *Discov. Nano* **2024**, *19*, 107. [CrossRef]
11. Hu, Q.; Solomon, P.; Österlund, L.; Zhang, Z. Nanotransistor-based gas sensing with record-high sensitivity enabled by electron trapping effect in nanoparticles. *Nat. Commun.* **2024**, *15*, 5259. [CrossRef]
12. Dey, A. Semiconductor metal oxide gas sensors: A review. *Mater. Sci. Eng. B* **2018**, *229*, 206–217. [CrossRef]
13. Goel, N.; Kunal, K.; Kushwaha, A.; Kumar, M. Metal oxide semiconductors for gas sensing. *Eng. Rep.* **2023**, *5*, e12604. [CrossRef]
14. He, Y.; Jiao, M. A Mini-Review on Metal Oxide Semiconductor Gas Sensors for Carbon Monoxide Detection at Room Temperature. *Chemosensors* **2024**, *12*, 55. [CrossRef]
15. Symons, E.A. Catalytic Gas Sensors. In *Gas Sensors: Principles, Operation and Developments*; Sberveglieri, G., Ed.; Springer: Dordrecht, The Netherlands, 1992; pp. 169–185. [CrossRef]
16. Gentry, S.J.; Jones, T.A. The role of catalysis in solid-state gas sensors. *Sens. Actuators* **1986**, *10*, 141–163. [CrossRef]
17. Wu, L.; Zhang, T.; Wang, H.; Tang, C.; Zhang, L. A Novel Fabricating Process of Catalytic Gas Sensor Based on Droplet Generating Technology. *Micromachines* **2019**, *10*, 71. [CrossRef] [PubMed]
18. Li, H.; Wu, R.; Liu, H.-B.; Han, L.-Y.; Yuan, W.-J.; Hua, Z.-Q.; Fan, S.-R.; Wu, Y. A novel catalytic-type gas sensor based on alumina ceramic substrates loaded with catalysts and printed electrodes. *Chin. J. Anal. Chem.* **2021**, *49*, 93–101. [CrossRef]
19. Williams, D.E. Electrochemical sensors for environmental gas analysis. *Curr. Opin. Electrochem.* **2020**, *22*, 145–153. [CrossRef]
20. Lakhmi, R.; Viricelle, J.-P.; Alrammouz, R.; Rieu, M. From the Modeling of an Electrochemical YSZ-Based Gas Sensor Used in Electrolysis Mode. *Sensors* **2024**, *24*, 658. [CrossRef]
21. Khan, M.A.H.; Rao, M.V.; Li, Q. Recent Advances in Electrochemical Sensors for Detecting Toxic Gases: NO_2, SO_2 and H_2S. *Sensors* **2019**, *19*, 905. [CrossRef]
22. Iliev, I.; Kaisheva, A. Electrochemical gas biosensors. In *Frontiers in Biosensorics II: Practical Applications*; Scheller, F.W., Schubert, F., Fedrowitz, J., Eds.; Birkhäuser: Basel, Switzerland, 1997; pp. 87–98. [CrossRef]
23. Dhall, S.; Mehta, B.R.; Tyagi, A.K.; Sood, K. A review on environmental gas sensors: Materials and technologies. *Sens. Int.* **2021**, *2*, 100116. [CrossRef]
24. Ariannejad, M.M.; Akbari, E.; Hanafi, E. Silicon sub-wavelength grating resonator structures for gas sensor. *Superlattices Microstruct.* **2020**, *142*, 106506. [CrossRef]
25. Shahbaz, M.; Butt, M.A.; Piramidowicz, R. Breakthrough in Silicon Photonics Technology in Telecommunications, Biosensing, and Gas Sensing. *Micromachines* **2023**, *14*, 1637. [CrossRef] [PubMed]
26. Chandra, V.; Ranjan, R. Performance analysis of different slot waveguide structures for evanescent field based gas sensor applications. *Opt. Quantum Electron.* **2021**, *53*, 457. [CrossRef]
27. Potyrailo, R.A.; Scherer, B.; Brewer, J.; Ruffalo, R. Boosting stability of photonic multi-gas sensors. In Proceedings of the 2022 IEEE Sensors, Dallas, TX, USA, 30 October–2 November 2022; pp. 1–4. [CrossRef]
28. Butt, M.A. Loop-Terminated Mach-Zehnder Interferometer Integrated with Functional Polymer for CO_2 Gas Sensing. *Appl. Sci.* **2024**, *14*, 4714. [CrossRef]
29. Aksnes, A. Photonic Sensors for Health and Environmental Monitoring. In *Sensors for Environment, Health and Security*; Baraton, M.-I., Ed.; Springer: Dordrecht, The Netherlands, 2009; pp. 191–203. [CrossRef]
30. Butt, M.A.; Voronkov, G.S.; Grakhova, E.P.; Kutluyarov, R.V.; Kazanskiy, N.L.; Khonina, S.N. Environmental Monitoring: A Comprehensive Review on Optical Waveguide and Fiber-Based Sensors. *Biosensors* **2022**, *12*, 1038. [CrossRef] [PubMed]
31. De, A.; Kalita, D. Bio-Fabricated Gold and Silver Nanoparticle Based Plasmonic Sensors for Detection of Environmental Pollutants: An Overview. *Crit. Rev. Anal. Chem.* **2023**, *53*, 672–688. [CrossRef] [PubMed]
32. Zhou, J.; Al Husseini, D.; Li, J.; Lin, Z.; Sukhishvili, S.; Coté, G.L.; Gutierrez-Osuna, R.; Lin, P.T. Detection of volatile organic compounds using mid-infrared silicon nitride waveguide sensors. *Sci. Rep.* **2022**, *12*, 5572. [CrossRef] [PubMed]
33. Butt, M.A.; Degtyarev, S.A.; Khonina, S.N.; Kazanskiy, N.L. An evanescent field absorption gas sensor at mid-IR 3.39 μm wavelength. *J. Mod. Opt.* **2017**, *64*, 1892–1897. [CrossRef]
34. Rose, J.J.; Wang, L.; Xu, Q.; McTiernan, C.F.; Shiva, S.; Tejero, J.; Gladwin, M.T. Carbon Monoxide Poisoning: Pathogenesis, Management, and Future Directions of Therapy. *Am. J. Respir. Crit. Care Med.* **2017**, *195*, 596–606. [CrossRef]

35. Ngoc, L.T.N.; Park, D.; Lee, Y.-C. Human Health Impacts of Residential Radon Exposure: Updated Systematic Review and Meta-Analysis of Case–Control Studies. *Int. J. Environ. Res. Public Health* **2023**, *20*, 97. [CrossRef]
36. David, E.; Niculescu, V.-C. Volatile Organic Compounds (VOCs) as Environmental Pollutants: Occurrence and Mitigation Using Nanomaterials. *Int. J. Environ. Res. Public Health* **2021**, *18*, 13147. [CrossRef]
37. Peterson, W.H.; Burris, R.H.; Sant, R.; Little, H.N. Toxic Gases in Silage, Production of Toxic Gas (Nitrogen Oxides) in Silage Making. *J. Agric. Food Chem.* **1958**, *6*, 121–126. [CrossRef]
38. Pangeni, R.P.; Timilsina, B.; Oli, P.R.; Khadka, S.; Regmi, P.R. A multidisciplinary approach to accidental inhalational ammonia injury: A case report. *Ann. Med. Surg.* **2022**, *82*, 104741. [CrossRef] [PubMed]
39. Bocci, V. Ozone as Janus: This Controversial Gas Can Be Either Toxic or Medically Useful. *Mediat. Inflamm.* **2004**, *13*, 3–11. [CrossRef] [PubMed]
40. Zhou, X.; Zhou, X.; Wang, C.; Zhou, H. Environmental and human health impacts of volatile organic compounds: A perspective review. *Chemosphere* **2023**, *313*, 137489. [CrossRef]
41. Jiang, J.; Chan, A.; Ali, S.; Saha, A.; Haushalter, K.J.; Lam, W.-L.M.; Glasheen, M.; Parker, J.; Brenner, M.; Mahon, S.B.; et al. Hydrogen Sulfide—Mechanisms of Toxicity and Development of an Antidote. *Sci. Rep.* **2016**, *6*, 20831. [CrossRef]
42. Anjana, N.S.; Amarnath, A.; Nair, M.V.H. Toxic hazards of ammonia release and population vulnerability assessment using geographical information system. *J. Environ. Manag.* **2018**, *210*, 201–209. [CrossRef]
43. Ho, W.F.; Chan, H.P.; Yang, K.L. Planar Optical Waveguide Platform for Gas Sensing Using Liquid Crystal. *IEEE Sens. J.* **2013**, *13*, 2521–2522. [CrossRef]
44. Vitoria, I.; Gallego, E.E.; Melendi-Espina, S.; Hernaez, M.; Zamarreño, C.R.; Matías, I.R. Gas Sensor Based on Lossy Mode Resonances by Means of Thin Graphene Oxide Films Fabricated onto Planar Coverslips. *Sensors* **2023**, *23*, 1459. [CrossRef]
45. Zheng, L.; Keppler, N.; Zhang, H.; Behrens, P.; Roth, B. Planar Polymer Optical Waveguide with Metal-Organic Framework Coating for Carbon Dioxide Sensing. *Adv. Mater. Technol.* **2022**, *7*, 2200395. [CrossRef]
46. Dominguez, I.; Del Villar, I.; Fuentes, O.; Corres, J.M.; Matias, I.R. Dually nanocoated planar waveguides towards multi-parameter sensing. *Sci. Rep.* **2021**, *11*, 3669. [CrossRef] [PubMed]
47. Barrios, C.A.; Bañuls, M.J.; González-Pedro, V.; Gylfason, K.B.; Sánchez, B.; Griol, A.; Maquieira, A.; Sohlström, H.; Holgado, M.; Casquel, R. Label-free optical biosensing with slot-waveguides. *Opt. Lett.* **2008**, *33*, 708–710. [CrossRef] [PubMed]
48. Butt, M.A.; Piramidowicz, R. Standard slot waveguide and double hybrid plasmonic waveguide configurations for enhanced evanescent field absorption methane gas sensing. *Photonics Lett. Pol.* **2022**, *14*, 10–12. [CrossRef]
49. Passaro, V.M.N.; Dell'Olio, F.; Ciminelli, C.; Armenise, M.N. Efficient Chemical Sensing by Coupled Slot SOI Waveguides. *Sensors* **2009**, *9*, 1012. [CrossRef] [PubMed]
50. Barrios, C.A. Optical Slot-Waveguide Based Biochemical Sensors. *Sensors* **2009**, *9*, 4751–4765. [CrossRef] [PubMed]
51. Ranacher, C.; Consani, C.; Jannesari, R.; Grille, T.; Jakoby, B. Numerical Investigations of Infrared Slot Waveguides for Gas Sensing. *Proceedings* **2018**, *2*, 799. [CrossRef]
52. Torrijos-Morán, L.; Griol, A.; García-Rupérez, J. Experimental study of subwavelength grating bimodal waveguides as ultrasensitive interferometric sensors. *Opt. Lett.* **2019**, *44*, 4702–4705. [CrossRef] [PubMed]
53. Awasthi, K.; Malviya, N.; Kumar, A. Silicon Subwavelength Grating Slot Waveguide based Optical Sensor for Label Free Detection of Fluoride Ion in Water. *IETE Tech. Rev.* **2024**, *41*, 341–352. [CrossRef]
54. Kazanskiy, N.L.; Khonina, S.N.; Butt, M.A. Subwavelength Grating Double Slot Waveguide Racetrack Ring Resonator for Refractive Index Sensing Application. *Sensors* **2020**, *20*, 3416. [CrossRef]
55. Tu, Z.; Gao, D.; Zhang, M.; Zhang, D. High-sensitivity complex refractive index sensing based on Fano resonance in the subwavelength grating waveguide micro-ring resonator. *Opt. Express* **2017**, *25*, 20911–20922. [CrossRef] [PubMed]
56. Arledge, K.E.; Uchoa, B.; Zou, Y.; Weng, B. Topological sensing with photonic arrays of resonant circular waveguides. *Phys. Rev. Res.* **2021**, *3*, 033106. [CrossRef]
57. Si, G.; Teo, E.J.; Bettiol, A.A.; Teng, J.; Danner, A.J. Suspended slab and photonic crystal waveguides in lithium niobate. *J. Vac. Sci. Technol. B* **2010**, *28*, 316–320. [CrossRef]
58. Butt, M.A.; Khonina, S.N.; Kazanskiy, N.L. Recent advances in photonic crystal optical devices: A review. *Opt. Laser Technol.* **2021**, *142*, 107265. [CrossRef]
59. Kassa-Baghdouche, L.; Cassan, E. Sensitivity analysis of ring-shaped slotted photonic crystal waveguides for mid-infrared refractive index sensing. *Opt. Quantum Electron.* **2019**, *51*, 328. [CrossRef]
60. Rostamian, A.; Midkiff, J.; Yoo, K.M.; Cheng, Y.; Chakravarty, S.; Chen, R. Mid-Infrared Trace Gas Sensing Using Photonic Crystal Waveguides. In Proceedings of the 2019 IEEE Photonics Society Summer Topical Meeting Series (SUM), Ft. Lauderdale, FL, USA, 8–10 July 2019; pp. 1–2. [CrossRef]
61. Peng, Z.; Huang, Y.; Zheng, K.; Zheng, C.; Pi, M.; Zhao, H.; Ji, J.; Min, Y.; Liang, L.; Song, F.; et al. Slow-light-enhanced on-chip 1D and 2D photonic crystal waveguide gas sensing in near-IR with an ultrahigh interaction factor. *Photonics Res.* **2023**, *11*, 1647–1656. [CrossRef]
62. Goyal, A.K.; Pal, S. Design and simulation of high sensitive photonic crystal waveguide sensor. *Optik* **2015**, *126*, 240–243. [CrossRef]
63. Butt, M.A.; Kazansky, N.L. SOI Suspended membrane waveguide at 3.39 μm for gas sensing application. *Photonics Lett. Pol.* **2020**, *12*, 67–69. [CrossRef]

64. Vlk, M.; Datta, A.; Alberti, S.; Murugan, G.S.; Aksnes, A.; Jágerská, J. Free-standing tantalum pentoxide waveguides for gas sensing in the mid-infrared. *Opt. Mater. Express* **2021**, *11*, 3111–3124. [CrossRef]
65. Yoo, K.M.; Midkiff, J.; Rostamian, A.; Chakravarty, S.; Chen, R.T. Suspended Membrane InGaAs Photonic Crystal Waveguides for ammonia sensing at λ = 6.15 μm. In Proceedings of the 2019 Conference on Lasers and Electro-Optics (CLEO), San Jose, CA, USA, 5–10 May 2019; Optica Publishing Group: San Jose, CA, USA, 2019; p. STh1F.6. [CrossRef]
66. Yoo, K.M.; Midkiff, J.; Rostamian, A.; Chung, C.; Dalir, H.; Chen, R.T. InGaAs Membrane Waveguide: A Promising Platform for Monolithic Integrated Mid-Infrared Optical Gas Sensor. *ACS Sens.* **2020**, *5*, 861–869. [CrossRef]
67. Butt, M.A.; Khonina, S.N.; Kazanskiy, N.L. Plasmonics: A Necessity in the Field of Sensing—A Review (Invited). *Fiber Integr. Opt.* **2021**, *40*, 14–47. [CrossRef]
68. Xu, Y.; Wang, F.; Gao, Y.; Zhang, D.; Sun, X.; Berini, P. Straight Long-Range Surface Plasmon Polariton Waveguide Sensor Operating at λ0 = 850 nm. *Sensors* **2020**, *20*, 2507. [CrossRef] [PubMed]
69. Kazanskiy, N.L.; Khonina, S.N.; Butt, M.A. Plasmonic sensors based on Metal-insulator-metal waveguides for refractive index sensing applications: A brief review. *Phys. E Low-Dimens. Syst. Nanostruct.* **2020**, *117*, 113798. [CrossRef]
70. Khonina, S.N.; Kazanskiy, N.L.; Butt, M.A.; Kaźmierczak, A.; Piramidowicz, R. Plasmonic sensor based on metal-insulator-metal waveguide square ring cavity filled with functional material for the detection of CO_2 gas. *Opt. Express* **2021**, *29*, 16584–16594. [CrossRef] [PubMed]
71. Joshi, K.; Meena, B.L.; Gehlot, K. Performance of silicon-on-insulator and silicon-on-sapphire based evanescent field gas sensor operating at 2.86 μm. *AIP Conf. Proc.* **2023**, *2768*, 020023. [CrossRef]
72. Butt, M.A.; Shahbaz, M.; Piramidowicz, R. Racetrack Ring Resonator Integrated with Multimode Interferometer Structure Based on Low-Cost Silica–Titania Platform for Refractive Index Sensing Application. *Photonics* **2023**, *10*, 978. [CrossRef]
73. Kazanskiy, N.L.; Butt, M.A.; Khonina, S.N. Carbon Dioxide Gas Sensor Based on Polyhexamethylene Biguanide Polymer Deposited on Silicon Nano-Cylinders Metasurface. *Sensors* **2021**, *21*, 378. [CrossRef] [PubMed]
74. Butt, M.A.; Kazanskiy, N.L.; Khonina, S.N. On-chip symmetrically and asymmetrically transformed plasmonic Bragg grating formation loaded with a functional polymer for filtering and CO_2 gas sensing applications. *Measurement* **2022**, *201*, 111694. [CrossRef]
75. Ma, W.; Xing, J.; Wang, R.; Rong, Q.; Zhang, W.; Li, Y.; Zhang, J.; Qiao, X. Optical Fiber Fabry–Perot Interferometric CO_2 Gas Sensor Using Guanidine Derivative Polymer Functionalized Layer. *IEEE Sens. J.* **2018**, *18*, 1924–1929. [CrossRef]
76. Kazanskiy, N.L.; Khonina, S.N.; Butt, M.A. Advancement in Silicon Integrated Photonics Technologies for Sensing Applications in Near-Infrared and Mid-Infrared Region: A Review. *Photonics* **2022**, *9*, 331. [CrossRef]
77. Song, Y.; Li, B.; Zhang, H.; Li, M.; Li, Q.; He, J.-J. Silicon Waveguide Sensors for Carbon Dioxide Gas Sensing in the Mid-Infrared Region. *Photonics* **2023**, *10*, 120. [CrossRef]
78. Butt, M.A. Dielectric Waveguide-Based Sensors with Enhanced Evanescent Field: Unveiling the Dynamic Interaction with the Ambient Medium for Biosensing and Gas-Sensing Applications—A Review. *Photonics* **2024**, *11*, 198. [CrossRef]
79. Khonina, S.N.; Kazanskiy, N.L.; Butt, M.A. Evanescent Field Ratio Enhancement of a Modified Ridge Waveguide Structure for Methane Gas Sensing Application. *IEEE Sens. J.* **2020**, *20*, 8469–8476. [CrossRef]
80. Consani, C.; Ranacher, C.; Tortschanoff, A.; Grille, T.; Irsigler, P.; Jakoby, B. Evanescent-Wave Gas Sensing Using an Integrated Thermal Light Source. *Proceedings* **2017**, *1*, 550. [CrossRef]
81. Butt, M.A.; Khonina, S.N.; Kazanskiy, N.L. Enhancement of evanescent field ratio in a silicon strip waveguide by incorporating a thin metal film. *Laser Phys.* **2019**, *29*, 076202. [CrossRef]
82. Vlk, M.; Datta, A.; Alberti, S.; Yallew, H.D.; Mittal, V.; Murugan, G.S.; Jágerská, J. Extraordinary evanescent field confinement waveguide sensor for mid-infrared trace gas spectroscopy. *Light Sci. Appl.* **2021**, *10*, 26. [CrossRef] [PubMed]
83. Ranacher, C.; Consani, C.; Vollert, N.; Tortschanoff, A.; Bergmeister, M.; Grille, T.; Jakoby, B. Characterization of Evanescent Field Gas Sensor Structures Based on Silicon Photonics. *IEEE Photonics J.* **2018**, *10*, 2700614. [CrossRef]
84. Wei, S.; Haggren, T.; Li, Z.; Tan, H.H.; Jagadish, C.; Tricoli, A.; Fu, L. Ultrasensitive Indium Phosphide Nanomembrane Wearable Gas Sensors. *Energy Environ. Mater.* **2024**, e12763. Available online: https://onlinelibrary.wiley.com/doi/full/10.1002/eem2.12763 (accessed on 7 June 2024). [CrossRef]
85. Rosborough, V.; Fridlander, J.; Sang, F.; Gambini, F.; Brunelli, S.T.; Chen, J.R.; Kawa, S.; Numata, K.; Stephen, M.; Coldren, L.; et al. Photonic Integration for Low Size, Weight, and Power (SWaP) Remote Gas Spectroscopy. In *OSA Optical Sensors and Sensing Congress 2021 (AIS, FTS, HISE, SENSORS, ES)*; Optica Publishing Group: Washington, DC, USA, 2021; p. ETu6D.2. [CrossRef]
86. Shahriar, R.; Hassan, O.; Alam, M.K. Adsorption of gas molecules on buckled GaAs monolayer: A first-principles study. *RSC Adv.* **2022**, *12*, 16732–16744. [CrossRef]
87. Xie, K.; Zhang, X.; Zhang, X.; Jin, H.; Jian, J. A slot microring sensor with feedback spiral waveguide for trace gas CH4 sensing in mid-infrared region. *Optoelectron. Lett.* **2019**, *15*, 1–5. [CrossRef]
88. Mere, V.; Selvaraja, S.K. Germanium-on-Glass Waveguides for Mid-IR Photonics. In *International Conference on Fibre Optics and Photonics*; Optica Publishing Group: Washington, DC, USA, 2016; p. Th3A-18. Available online: https://opg.optica.org/abstract.cfm?uri=photonics-2016-Th3A.18 (accessed on 31 January 2024).
89. Soref, R. Mid-Infrared Photonics in Silicon and Germanium. *Nat. Photonics* **2010**, *4*, 495–497. [CrossRef]
90. Kim, S.; Han, J.H.; Shim, J.P.; Kim, H.J.; Choi, W.J. Verification of Ge-on-Insulator Structure for a Mid-Infrared Photonics Platform. *Opt. Mater. Express* **2018**, *8*, 440–451. [CrossRef]

91. Dong, M.; Zheng, C.; Miao, S.; Zhang, Y.; Du, Q.; Wang, Y.; Tittel, F.K. Development and Measurements of a Mid-Infrared Multi-Gas Sensor System for CO, CO_2 and CH_4 Detection. *Sensors* **2017**, *17*, 2221. [CrossRef] [PubMed]
92. Yebo, N.A.; Lommens, P.; Hens, Z.; Baets, R. An Integrated Optic Ethanol Vapor Sensor Based on a Silicon-on-Insulator Microring Resonator Coated with a Porous ZnO Film. *Opt. Express* **2010**, *18*, 11859–11866. [CrossRef] [PubMed]
93. Jin, T.; Zhou, J.; Tai, P. Real-time and non-destructive hydrocarbon gas sensing using mid-infrared integrated photonic circuits. *RSC Adv.* **2020**, *10*, 7452–7459. [CrossRef] [PubMed]
94. Kazanskiy, N.L.; Khonina, S.N.; Butt, M.A. Polarization-Insensitive Hybrid Plasmonic Waveguide Design for Evanescent Field Absorption Gas Sensor. *Photonic Sens.* **2021**, *11*, 279–290. [CrossRef]
95. Butt, M.A.; Khonina, S.N.; Kazanskiy, N.L. Modelling of Rib channel waveguides based on silicon-on-sapphire at 4.67 μm wavelength for evanescent field gas absorption sensor. *Optik* **2018**, *168*, 692–697. [CrossRef]
96. Mi, G.; Horvath, C.; Van, V. Silicon photonic dual-gas sensor for H_2 and CO_2 detection. *Opt. Express* **2017**, *25*, 16250–16259. [CrossRef] [PubMed]
97. Wang, W.-Y.; Hu, H.-W.; Chiou, J.-C.; Yung, K.-F.; Kan, C.-W. Poly(hexamethylene biguanide) hydrochloride (PHMB)-based materials: Synthesis, modification, properties, determination, and application. *Polym. Chem.* **2023**, *14*, 5226–5252. [CrossRef]
98. Silicon Microring Refractometric Sensor for Atmospheric CO_2 Gas Monitoring'. Available online: https://opg.optica.org/oe/fulltext.cfm?uri=oe-24-2-1773&id=335762 (accessed on 4 May 2024).
99. Virji, S.; Huang, J.; Kaner, R.B.; Weiller, B.H. Polyaniline Nanofiber Gas Sensors: Examination of Response Mechanisms. *Nano Lett.* **2004**, *4*, 491–496. [CrossRef]
100. Kroutil, J.; Laposa, A.; Povolny, V.; Klimsa, L.; Husak, M. Gas Sensor with Different Morphology of PANI Layer. *Sensors* **2023**, *23*, 1106. [CrossRef] [PubMed]
101. Fratoddi, I.; Venditti, I.; Cametti, C.; Russo, M.V. Chemiresistive polyaniline-based gas sensors: A mini review. *Sens. Actuators B Chem.* **2015**, *220*, 534–548. [CrossRef]
102. Jain, A.; Nabeel, A.N.; Bhagwat, S.; Kumar, R.; Sharma, S.; Kozak, D.; Hunjet, A.; Kumar, A.; Singh, R. Fabrication of polypyrrole gas sensor for detection of NH_3 using an oxidizing agent and pyrrole combinations: Studies and characterizations. *Heliyon* **2023**, *9*, e17611. [CrossRef] [PubMed]
103. Li, W.; Lefferts, M.J.; Armitage, B.I.; Murugappan, K.; Castell, M.R. Polypyrrole Percolation Network Gas Sensors: Improved Reproducibility through Conductance Monitoring during Polymer Growth. *ACS Appl. Polym. Mater.* **2022**, *4*, 2536–2543. [CrossRef] [PubMed]
104. Bhatt, C.M.; Jampana, N. Comparative studies on electrical properties of Polypyrrole based gas sensor. In Proceedings of the 2011 IEEE Sensors Applications Symposium, San Antonio, TX, USA, 22–24 February 2011; pp. 131–135. [CrossRef]
105. Nagashima, K.; Kamaya, M.; Ishii, E. Electrochemical gas sensors using electrolytic films of poly(ethylene oxide)/Zn, Cu, Ni trifluoromethane sulphonates for flow injection analysis of nitrogen dioxide. *Sens. Actuators B Chem.* **1992**, *9*, 149–154. [CrossRef]
106. Nagashima, K.; Meguro, K.; Hobo, T. A galvanic gas sensor using poly (ethylene oxide) complex of silver trifluoromethane sulphonate electrolyte. *Fresenius J. Anal. Chem.* **1990**, *336*, 571–574. [CrossRef]
107. Khanloo, A.S.H.; Sarraf, M.J.; Rostami, A.; Dolatyari, M. Micro ring CO_2 gas sensor using PbSe quantum dots. *Opt. Quantum Electron.* **2023**, *55*, 882. [CrossRef]
108. Zhang, G.; Feng, X.L.; Liedberg, B.; Liu, A.Q. Gas Sensor for Volatile Organic Compounds Detection Using Silicon Photonic Ring Resonator. *Procedia Eng.* **2016**, *168*, 1771–1774. [CrossRef]
109. Zhao, H.; Du, J.; Wang, S.; Wang, X.; Zhang, T.; Yu, R.; Chi, Z.; Wang, B. Triple narrow-spectrum enhanced multiparameter sensor based on asymmetric MIM waveguide for gas and liquid sensing. *Opt. Laser Technol.* **2024**, *175*, 110754. [CrossRef]
110. Kazanskiy, N.L.; Khonina, S.N.; Butt, M.A. Recent Development in Metasurfaces: A Focus on Sensing Applications. *Nanomaterials* **2023**, *13*, 118. [CrossRef]
111. Chatterjee, S.; Shkondin, E.; Takayama, O.; Fisher, A.; Fraiwan, A.; Gurkan, U.A.; Lavrinenko, A.V.; Strangi, G. Hydrogen gas sensing using aluminum doped ZnO metasurfaces. *Nanoscale Adv.* **2020**, *2*, 3452–3459. [CrossRef] [PubMed]
112. Butt, M.A.; Khonina, S.N.; Kazanskiy, N.L.; Piramidowicz, R. Hybrid metasurface perfect absorbers for temperature and biosensing applications. *Opt. Mater.* **2022**, *123*, 111906. [CrossRef]
113. Nugroho, F.A.A.; Bai, P.; Darmadi, I.; Castellanos, G.W.; Fritzsche, J.; Langhammer, C.; Rivas, J.G.; Baldi, A. Inverse designed plasmonic metasurface with parts per billion optical hydrogen detection. *Nat. Commun.* **2022**, *13*, 5737. [CrossRef] [PubMed]
114. Danila, O.; Gross, B.M. Towards Highly Efficient Nitrogen Dioxide Gas Sensors in Humid and Wet Environments Using Triggerable-Polymer Metasurfaces. *Polymers* **2023**, *15*, 545. [CrossRef] [PubMed]
115. Meng, J.; Balendhran, S.; Sabri, Y.; Bhargava, S.K.; Crozier, K.B. Smart mid-infrared metasurface microspectrometer gas sensing system. *Microsyst. Nanoeng.* **2024**, *10*, 74. [CrossRef] [PubMed]
116. Kim, I.; Kim, W.-S.; Kim, K.; Ansari, M.A.; Mehmood, M.Q.; Badloe, T.; Kim, Y.; Gwak, J.; Lee, H.; Kim, Y.-K.; et al. Holographic metasurface gas sensors for instantaneous visual alarms. *Sci. Adv.* **2021**, *7*, eabe9943. [CrossRef] [PubMed]
117. Tabassum, S.; Nayemuzzaman, S.; Kala, M.; Kumar Mishra, A.; Mishra, S.K. Metasurfaces for Sensing Applications: Gas, Bio and Chemical. *Sensors* **2022**, *22*, 6896. [CrossRef] [PubMed]
118. Kazanskiy, N.L.; Khonina, S.N.; Butt, M.A. Metasurfaces: Shaping the future of photonics. *Sci. Bull.* **2024**, *69*, 1607–1611. [CrossRef] [PubMed]

119. Warken, F.; Vetsch, E.; Meschede, D.; Sokolowski, M.; Rauschenbeutel, A. Ultra-sensitive surface absorption spectroscopy using sub-wavelength diameter optical fibers. *Opt. Express* **2007**, *15*, 11952–11958. [CrossRef]
120. Potyrailo, R.A.; Hobbs, S.E.; Hieftje, G.M. Near-Ultraviolet Evanescent-Wave Absorption Sensor Based on a Multimode Optical Fiber. *Anal. Chem.* **1998**, *70*, 1639–1645. [CrossRef]
121. Benito-Peña, E.; Valdés, M.G.; Glahn-Martínez, B.; Moreno-Bondi, M.C. Fluorescence based fiber optic and planar waveguide biosensors. A review. *Anal. Chim. Acta* **2016**, *943*, 17–40. [CrossRef] [PubMed]
122. Epstein, J.R.; Walt, D.R. Fluorescence-based fibre optic arrays: A universal platform for sensing. *Chem. Soc. Rev.* **2003**, *32*, 203–214. [CrossRef] [PubMed]
123. Ding, L.; Gong, P.; Xu, B.; Ding, Q. An Optical Fiber Sensor Based on Fluorescence Lifetime for the Determination of Sulfate Ions. *Sensors* **2021**, *21*, 954. [CrossRef] [PubMed]
124. Thompson, R.B. Fluorescence-Based Fiber-Optic Sensors. In *Topics in Fluorescence Spectroscopy: Principles*; Lakowicz, J.R., Ed.; Springer: Boston, MA, USA, 2002; pp. 345–365. [CrossRef]
125. Wolfbeis, O.S.; Posch, H.E. Fibre-optic fluorescing sensor for ammonia. *Anal. Chim. Acta* **1986**, *185*, 321–327. [CrossRef]
126. Zhang, C.; Liu, Z.; Cai, C.; Yang, Z.; Qi, Z.-M. Surface plasmon resonance gas sensor with a nanoporous gold film. *Opt. Lett.* **2022**, *47*, 4155–4158. [CrossRef]
127. Zhao, H.; Wang, F.; Han, Z.; Cheng, P.; Ding, Z. Research Advances on Fiber-Optic SPR Sensors with Temperature Self-Compensation. *Sensors* **2023**, *23*, 644. [CrossRef] [PubMed]
128. Allsop, T.; Neal, R. A Review: Application and Implementation of Optic Fibre Sensors for Gas Detection. *Sensors* **2021**, *21*, 6755. [CrossRef] [PubMed]
129. Chen, X.; Gan, L.; Guo, X. Optical Fiber-Based Gas Sensing for Early Warning of Thermal Runaway in Lithium-Ion Batteries. *Adv. Sens. Res.* **2023**, *2*, 2300055. [CrossRef]
130. Xiong, S.; Yin, X.; Wang, Q.; Xia, J.; Chen, Z.; Lei, H.; Yan, X.; Zhu, A.; Qiu, F.; Chen, B.; et al. Photoacoustic Spectroscopy Gas Detection Technology Research Progress. *Appl. Spectrosc.* **2024**, *78*, 139–158. [CrossRef]
131. Yang, T.; Chen, W.; Wang, P. A review of all-optical photoacoustic spectroscopy as a gas sensing method. *Appl. Spectrosc. Rev.* **2021**, *56*, 143–170. [CrossRef]
132. Zhang, X.; Liu, L.; Zhang, L.; Yin, X.; Huan, H.; Zhang, L.; Shao, X. A compact portable photoacoustic spectroscopy sensor for multiple trace gas detection. *J. Appl. Phys.* **2022**, *131*, 174501. [CrossRef]
133. Qiao, S.; He, Y.; Sun, H.; Patimisco, P.; Sampaolo, A.; Spagnolo, V.; Ma, Y. Ultra-highly sensitive dual gases detection based on photoacoustic spectroscopy by exploiting a long-wave, high-power, wide-tunable, single-longitudinal-mode solid-state laser. *Light Sci. Appl.* **2024**, *13*, 100. [CrossRef]
134. Qiao, S.; Qu, Y.; Ma, Y.; He, Y.; Wang, Y.; Hu, Y.; Yu, X.; Zhang, Z.; Tittel, F.K. A Sensitive Carbon Dioxide Sensor Based on Photoacoustic Spectroscopy with a Fixed Wavelength Quantum Cascade Laser. *Sensors* **2019**, *19*, 4187. [CrossRef] [PubMed]
135. Wang, Z.L.; Tian, C.W.; Liu, Q.; Chang, J.; Zhang, Q.D.; Zhu, C.G. Wavelength modulation technique-based photoacoustic spectroscopy for multipoint gas sensing. *Appl. Opt.* **2018**, *57*, 2909–2914. [CrossRef]
136. Elia, A.; Di Franco, C.; Lugarà, P.M.; Scamarcio, G. Photoacoustic Spectroscopy with Quantum Cascade Lasers for Trace Gas Detection. *Sensors* **2006**, *6*, 1411. [CrossRef]
137. Patimisco, P.; Scamarcio, G.; Tittel, F.K.; Spagnolo, V. Quartz-Enhanced Photoacoustic Spectroscopy: A Review. *Sensors* **2014**, *14*, 6165. [CrossRef]
138. Hänsel, A.; Heck, M.J.R. Feasibility of Telecom-Wavelength Photonic Integrated Circuits for Gas Sensors. *Sensors* **2018**, *18*, 2870. [CrossRef]
139. Hänsel, A.; Adamu, A.I.; Markos, C.; Feilberg, A.; Bang, O.; Heck, M.J.R. Integrated Ammonia Sensor Using a Telecom Photonic Integrated Circuit and a Hollow Core Fiber. *Photonics* **2020**, *7*, 93. [CrossRef]
140. Butt, M.A. Integrated Optics: Platforms and Fabrication Methods. *Encyclopedia* **2023**, *3*, 824–838. [CrossRef]
141. Liaros, N.; Fourkas, J.T. Ten years of two-color photolithography [Invited]. *Opt. Mater. Express* **2019**, *9*, 3006. [CrossRef]
142. Crowell, J.E. Chemical methods of thin film deposition: Chemical vapor deposition, atomic layer deposition, and related technologies. *J. Vac. Sci. Technol. A* **2003**, *21*, S88–S95. [CrossRef]
143. Joyce, B.A. Molecular beam epitaxy-fundamentals and current status. *Contemp. Phys.* **1990**, *31*, 195–197. [CrossRef]
144. Butt, M.A.; Tyszkiewicz, C.; Karasiński, P.; Zięba, M.; Hlushchenko, D.; Baraniecki, T.; Kazmierczak, A.; Piramidowicz, R.; Guzik, M.; Bachmatiuk, A. Development of a low-cost silica-titania optical platform for integrated photonics applications. *Opt. Express* **2022**, *30*, 23678. [CrossRef] [PubMed]
145. Butt, M.A.; Tyszkiewicz, C.; Wojtasik, K.; Karasiński, P.; Kaźmierczak, A.; Piramidowicz, R. Subwavelength Grating Waveguide Structures Proposed on the Low-Cost Silica–Titania Platform for Optical Filtering and Refractive Index Sensing Applications. *Int. J. Mol. Sci.* **2022**, *23*, 6614. [CrossRef] [PubMed]
146. Ober, C.K.; Käfer, F.; Yuan, C. Recent developments in photoresists for extreme-ultraviolet lithography. *Polymer* **2023**, *280*, 126020. [CrossRef]
147. Aassime, A.; Hamouda, F. Conventional and Un-Conventional Lithography for Fabricating Thin Film Functional Devices. In *Modern Technologies for Creating the Thin-Film Systems and Coatings*; IntechOpen: London, UK, 2017. Available online: https://www.intechopen.com/chapters/53135 (accessed on 5 July 2024).

148. Chen, Y. Nanofabrication by electron beam lithography and its applications: A review. *Microelectron. Eng.* **2015**, *135*, 57–72. [CrossRef]
149. Hohn, F.J. Electron beam lithography: Its applications. *J. Vac. Sci. Technol. B Microelectron. Process. Phenom.* **1989**, *7*, 1405–1411. [CrossRef]
150. Ferstl, M. Reactive ion etching: A versatile fabrication technique for micro-optical elements. In *Diffractive Optics and Micro-Optics*; Optica Publishing Group: Kailua-Kona, HI, USA, 1998; p. DTuD.21. [CrossRef]
151. Schmitt, J.; Meier, A.; Wallrabe, U.; Völklein, F. Reactive ion etching (CF4/Ar) and ion beam etching of various glasses for diffractive optical element fabrication. *Int. J. Appl. Glass Sci.* **2018**, *9*, 499–509. [CrossRef]
152. Tolpygo, S.K.; Bolkhovsky, V.; Weir, T.J.; Wynn, A.; Oates, D.E.; Johnson, L.M.; Gouker, M.A. Advanced Fabrication Processes for Superconducting Very Large-Scale Integrated Circuits. *IEEE Trans. Appl. Supercond.* **2016**, *26*, 1–10. [CrossRef]
153. Morrison, S.R. Selectivity in semiconductor gas sensors. *Sens. Actuators* **1987**, *12*, 425–440. [CrossRef]
154. Tonezzer, M.; Izidoro, S.C.; Moraes, J.P.A.; Dang, L.T.T. Improved Gas Selectivity Based on Carbon Modified SnO_2 Nanowires. *Front. Mater.* **2019**, *6*, 277. [CrossRef]
155. Barik, P.; Pradhan, M. Selectivity in trace gas sensing: Recent developments, challenges, and future perspectives. *Analyst* **2022**, *147*, 1024–1054. [CrossRef] [PubMed]
156. Wang, H.; Feng, Z.; Zhang, Y.; Han, D.; Ma, J.; Chai, X.; Sang, S. Highly sensitive and low detection limit NO_2 gas sensor based on In_2O_3 nanoparticles modified peach kernel-like GaN composites. *Sens. Actuators B Chem.* **2023**, *382*, 133452. [CrossRef]
157. Hänsel, A.; Heck, M.J.R. Opportunities for photonic integrated circuits in optical gas sensors. *J. Phys. Photonics* **2020**, *2*, 012002. [CrossRef]
158. Qin, J.; Jiang, S.; Wang, Z.; Cheng, X.; Li, B.; Shi, Y.; Tsai, D.P.; Liu, A.Q.; Huang, W.; Zhu, W. Metasurface Micro/Nano-Optical Sensors: Principles and Applications. *ACS Nano* **2022**, *16*, 11598–11618. [CrossRef]
159. Allsop, T.; Arif, R.; Neal, R.; Kalli, K.; Kundrát, V.; Rozhin, A.; Culverhouse, P.; Webb, D.J. Photonic gas sensors exploiting directly the optical properties of hybrid carbon nanotube localized surface plasmon structures. *Light Sci. Appl.* **2016**, *5*, e16036. [CrossRef]